Hadron Physics

The production of strange hadrons and electromagnetic radiation from colliding hadron systems allows insights in the properties of dense nuclear matter as formed in violent cosmic processes like super-novae and as present in a certain phase of the big bang. In particular, the experimental research of the department focuses on in-medium modifications of hadrons, i. e. their behavior when embedded in strongly interacting matter. Various heavy-ion experiments in the 1 GeV range point to such changes in a medium. For instance, dedicated measurements by the KaoS and FOPI collaborations at the heavy-ion synchrotron SIS in Darmstadt can be interpreted by a slight mass enhancement of kaons and a significant mass reduction of anti-kaons. While these interesting findings can be attributed to an evidence for partial restoration of chiral symmetry in dense nuclear matter produced in the course of heavy-ion collisions, other interpretations are conceivable, too.

In this respect the measurements of kaon production in proton-nucleus collisions represent the missing link for systematically understanding strangeness production. During the last years the COSY-11 and TOF collaborations at the cooler synchrotron COSY in Jülich enlarged already the data basis for strangeness production in elementary hadron reactions. Now the final analysis of the experiments by the KaoS collaboration at SIS and the ANKE collaboration at COSY is eagerly waited for. Both experiments measure in complementary phase space regions kaons produced by a proton beam at various energies impinging on various target nuclei.

Hidden strangeness, e. g. in ϕ mesons, represents another facet of strangeness degrees of freedom. While ϕ production is presently a hot topic in hadron reactions with respect to the strangeness sea in nucleons and OZI rule violations, the ϕ multiplicity in heavy-ion collisions appears puzzling. The analysis of data taken previously with the FOPI detector points to a ϕ production probability being much larger than can be understood within the framework of transport models.

While selected hadron channels, in particular these with strangeness, are sensitive to in-medium effects, a direct measurement of spectral functions is desirable. This goal can be accomplished, e. g., via the dielectron decay channels. Indeed, the starting HADES project at SIS is aimed at studying the in-medium properties of ρ, ω and ϕ mesons in a nuclear environment. Since the fall of 2000, HADES is operating and begins with data taking while being completed. The first multi-wire chamber built in our detector workshop has proven to work successfully. The remaining 5 chambers from Rossendorf will be installed in the HADES detector system during 2001 thus enabling, together with the other chambers, the required high-precision resolution of charged particles tracks. HADES is expected to have a large scientific potential for various investigations with the pion, proton and heavy-ion beams delivered at the SIS.

The theory group in the hadron physics department is accompanying these experimental activities. Predictions and interpretations of selected topics in the realm of strange and rare electromagnetic probes are provided. Most of these calculations refer to the energy range covered by the experiments performed with FZR participation (see collaboration list below), others deal with various phenomenological aspects of deconfined matter, as a state with chiral symmetry restoration in the strongly interacting medium, produced in high-energy heavy-ion reactions. Whereas the investigations of dense and hot hadronic matter as produced in medium-energy collisions are of strong interest for the understanding of astronomical objects like supernovae and neutron stars, the quark-gluon phase transition studies are of relevance for more violent scenarios like the big bang.

Collaborations

<u>ANKE:</u> *Univ. Münster, FZ Jülich, Univ. Giessen, Univ. Bonn, Univ. Köln, Univ. Erlangen- Nürnberg, Fachhochschule München, FZ Rossendorf, JINR Dubna (Russia), Univ. Tblisi (Georgia), Petersburg Nuclear Physics Institute (Russia), ITEP Moscow (Russia), Russian Academy of Science Moscow (Russia), ECN-Nuclear Energy (Netherlands), Jagellonian Univ. Cracow (Poland), Moscow State University (Russia), Univ. College London (England), Soltan Institute for Nuclear Studies (Poland),*
spokesperson: K. Sistemich

<u>FOPI:</u> *Univ. Heidelberg, GSI Darmstadt, FZ Rossendorf, IPNE Bucharest (Romania), KFKI Budapest (Hungary), LPC and Univ. Blaise Pascal Clermont (France), ITEP Moscow (Russia), Kurchatov Institute Moscow (Russia), Korea Univ. Seoul (South Korea), IreS Strasbourg (France), Univ. Warsaw (Poland), RBI Zagreb (Croatia),*
spokesperson: N. Herrmann

<u>HADES:</u> *Univ. Frankfurt, TU München, Univ. Giessen, GSI Darmstadt, FZ Rossendorf, Institute of Physics Bratislava (Slovakia), LNS Catania (Italy), LPC and Univ. Blaise Pascal Clermont (France), Jagellonian Univ. Cracow (Poland), JINR Dubna (Russia), Univ. degli Studi di Milano (Italy), ITEP Moscow (Russia), INR Moscow (Russia), MEPhI Moscow (Russia), Univ. of Cyprus (Cyprus), Institute de Physique Nucleaire d'Orsay (France), Nuclear Physics Institute Rez (Tschechia), Univ. of Santiago de Compostela (Spain), Univ. of Valencia (Spain),*
spokesperson: J. Friese

<u>KaoS:</u> *TU Darmstadt, Univ. Frankfurt, Univ. Marburg, GSI Darmstadt, Jagellonian Univ. Cracow (Poland), FZ Rossendorf,*
spokesperson: P. Senger

<u>TOF:</u> *Univ. Bochum, FZ Jülich, Univ. Bonn, TU Dresden, Fachhochschule Jülich, Univ. Tübingen, Univ. Erlangen-Nürnberg, FZ Rossendorf, IUCF Bloomington (USA), INFN Torino (Italy), SINS Warsaw (Poland),*
local organizer: E. Roderburg

Kaon and Antikaon Production in Proton-Nucleus Collisions [G]

W. Scheinast[1] for the KaoS collaboration:
I. Böttcher[4], M. Dębowski[1], F. Dohrmann*, A. Förster[3], E. Grosse[7], B. Kamys[6], P. Koczoń[2], B. Kohlmeyer[4], F. Laue**, M. Menzel[4], L. Naumann[1], H. Oeschler[3], F. Pühlhofer[4], Ch. Schneider[1], E. Schwab[2], P. Senger[2], Y. Shin[5], H. Ströbele[5], Ch. Sturm[3], G. Surówka[6], F. Uhlig[3], A. Wagner[1], W. Waluś[6]

During the last year the analysis of the data on K^+ and K^- production in proton-nucleus collisions has continued and now first results can be presented. The experiment already described in the last annual report had taken place 1998 at SIS/GSI Darmstadt. In the kaon spectrometer a new 2nd level trigger enabled beam intensities above $10^9\,s^{-1}$ to be applied.

Fig. 1 shows double differential cross sections for $K^\pm$ production. The 3.5 GeV data exhibit structures which might be caused by a yet unknown problem with the trigger efficiency (the trigger was different for the 2.5 GeV data).

In the 2.5 GeV K^+ spectra the maximum of the differential cross section shifts to lower momenta with increasing mass number. Taking into account the observation angle of 40°, this is an evidence for the emission system being different in these targets. The K^+ are emitted more towards target rapidity in the p+Au system. Consequently they are either produced in secondary reactions or rescattered before leaving the nucleus.

Heavy ion data at comparable energies can well be described by Boltzmann distributions (e. g. in [1]). When trying this for the proton data, one has to know the kaon emission frame. Fig. 1 contains the fits of the 2.5 GeV spectra with a Boltzmann function in the proton-nucleus center-of-mass frame. An attempt to adjust this distribution in the nucleon-nucleon frame failed. This can be regarded as a hint for the K^+ being produced in multistep processes. The inverse slope parameters are $T = 123.5(9)$ MeV (Au) and $T = 115.5(8)$ MeV (C).

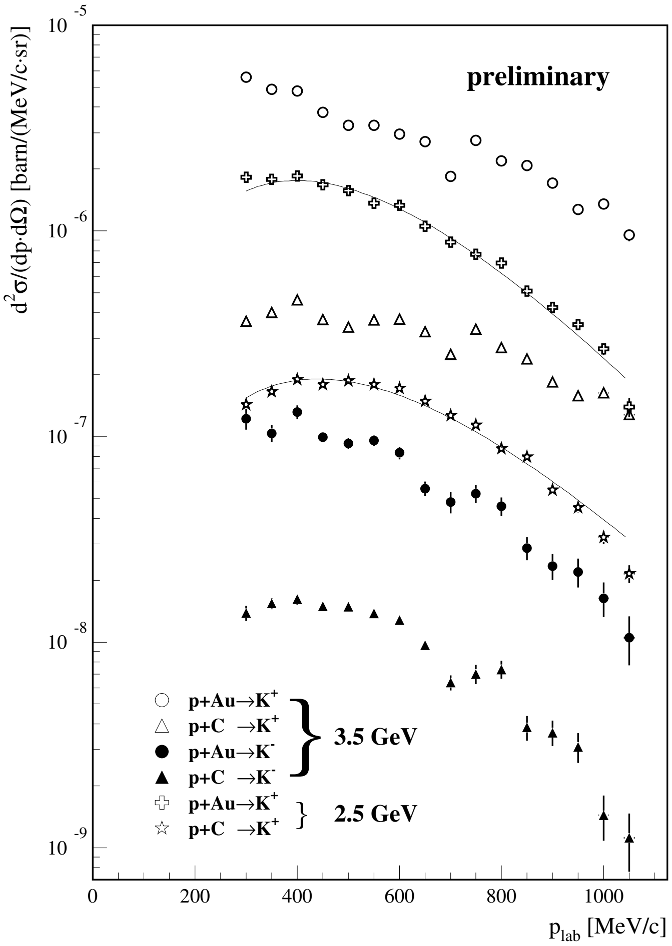

Fig. 1 Inclusive double differential K-meson production cross sections versus momentum in the laboratory frame at a polar angle of 40°. Only statistical errors are plotted. Open symbols denote K^+, full symbols K^-.

K^+ are scarcely absorbed in nuclear matter because strangeness exchange reactions are not possible. Antikaons do these reactions, e. g. $K^- + N \rightarrow \pi + \Lambda$, so they are strongly absorbed. In Fig. 2 two K^-/K^+ ratios at 3.5 GeV are plotted. The difference between carbon and gold target might be a hint for K^- absorption, but can also arise from a difference in the emission systems between K^+ and K^-.

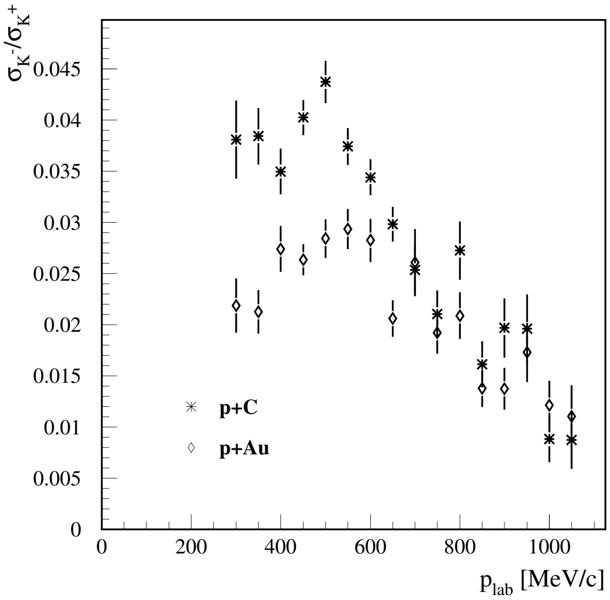

Fig. 2 *K^-/K^+ ratio at 3.5 GeV, from the spectra of Fig. 1.*

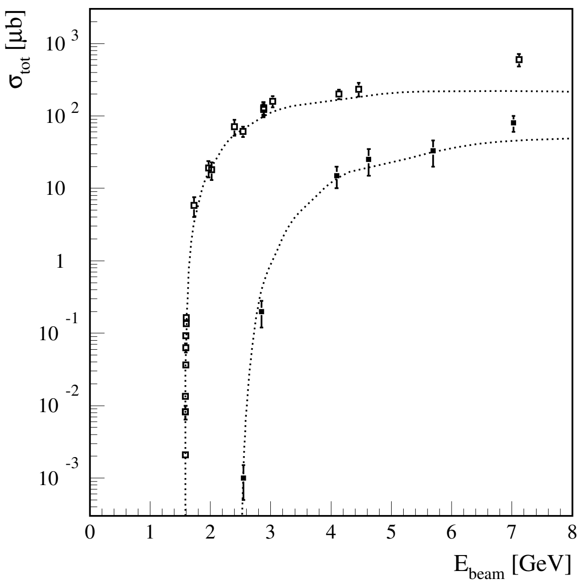

Fig. 3 *Compilation [2] of total cross sections on K^+ (left curve) and K^- (right curve) production in p+p collisions. The curves represent parametrizations [4].*

Over the shown momentum range this ratio is in the same order of magnitude as the ratio of total p+p cross sections, as can be seen in Fig. 3. So, the 3.5 GeV data seem not to exhibit obvious in-medium effects besides rescattering and absorption. If there are such effects, they must be visible more clearly in near-threshold data, i. e. 1.6 and 2.5 GeV. The future analysis will show this and will allow a comparison to complementary data from ITEP[3] and COSY/ANKE.

[1] *FZR*
[2] *GSI Darmstadt*
[3] *TU Darmstadt, Institut für Kernphysik*
[4] *Universität Marburg, Physikalisches Institut*
[5] *Universität Frankfurt, Institut für Kernphysik*
[6] *Jagiellonian University Cracow, Institute of Physics, Poland*
[7] *FZR and TU Dresden, Institut für Kern- und Teilchenphysik*
[*] *FZR, now at Argonne National Laboratory, Argonne IL, USA*
[**] *GSI, now at Ohio State University, Columbus OH, USA*

References

[1] C. Sturm et al., Phys. Rev. Lett. 86/1 (2001) 39
[2] P. Senger, H. Ströbele, J. Phys. G 25 (1999) R59
[3] Y. T. Kiselev et al., J. Phys. G 25 (1999) 381
[4] A. Sibirtsev, Phys. Lett. B 359 (1995) 29,
A. Sibirtsev et al., Z. Phys. A 358 (1997) 101

Centrality Dependence of Kaon and Antikaon Production in Ni+Ni Collisions at SIS Energies [B,G]

M. Menzel[4], I.M. Böttcher[4], M. Dębowski[5,6], F. Dohrmann[6], A. Förster[2], E. Grosse[6,7], P. Koczoń[1], B. Kohlmeyer[4], F. Laue[1,*], L. Naumann[6], H. Oeschler[2], F. Pühlhofer[4], W. Scheinast[6], E. Schwab[1], P. Senger[1], Y. Shin[3], H. Ströbele[3], C. Sturm[2], G. Surówka[5], F. Uhlig[2], A. Wagner[6], W. Waluś[5]

Kaons and antikaons are regarded as a promising probe to study hadron properties in dense nuclear matter. Recent experimental results obtained with the Kaon Spectrometer indicate modifications of the in-medium properties of K^+ and K^-. Remarkable results are that the K^-/K^+ ratio is enhanced compared to pp collisions [1,2,3], the spectral slope for the antikaons is steeper than for the kaons [2] and a preferential out-of-plane emission of K^+ is observed [4].
In order to study the kaon production as a function of the reaction centrality and the beam energy, we have measured K^+ and K^- mesons around midrapidity ($\theta_{lab} = 40° \pm 4°$) in Ni+Ni reactions at beam energies of 1.1 (K^+ only), 1.5 and 1.93 AGeV. The multiplicity of charged particles measured by a target hodoscope is used to determine the centrality. The data set is subdivided in five centrality bins MUL1 to MUL5 for each beam energy. From a measurement under minimum bias conditions the reaction cross section is determined. For all beam energies we find a reaction cross section of $\sigma_R = 2.9 \pm 0.3$ barn, which agrees with the geometric model. The relative reaction cross section for each centrality class $\sigma_{R,MUL}/\sigma_R$ is given in Table 1 for 1.5 and 1.93 AGeV. Errors of about 10 % have to be added to the ratio $\sigma_{R,MUL}/\sigma_R$.
Figure 1 shows the invariant cross sections of K^+ (full circles) and K^- (open circles) for central to peripheral collisions (see middle panel: MUL 5 to MUL 1) as a function of the center-of-mass kinetic energy at beam energies of 1.1, 1.5 and 1.93 AGeV. The K^- mesons are scaled by a factor of 20 (see lower panel) and the yields in the bins are scaled by factors of 10 (see upper panel). The error bars shown are due to statistics only and a systematic error of 10% has to be added, caused by beam normalization, acceptance determination and trigger efficiency. The lines represent Boltzmann distributions $d^3\sigma/dp^3 \propto exp(-E_{CM}/T)$ fitted to the spectra individually for each multiplicity bin. The integrated kaon cross sections $4\pi(d\sigma_K/d\Omega_{CM})$ and the inverse slope parameters T as a function of the centrality are given in Table 1 for 1.5 and 1.93 AGeV. The errors of both quantities include the systematic effects. For all beam energies the spectral slopes decrease (Figure 1) and the inverse slope parameters T increase (Table 1) with increasing centrality of the reaction for both, kaons and antikaons. We determined the average multiplicity per number of participating nucleons M_K/A_{part} as a function of the number of participating nucleons. M_K is calculated via $M_K = \sigma_K/\sigma_{R,MUL}$ with $\sigma_K = 4\pi(d\sigma_K/d\Omega_{CM})$ and with the reaction cross section for each multiplicity class $\sigma_{R,MUL}$. A_{part} is calculated from the number of nucleons in the overlap of the colliding nuclei. The impact parameter b is determined for the center of each multiplicity bin. The kaon and antikaon multiplicity per A_{part} (full circles: K^+, open: K^-) is shown in Figure 2 (different scaling factors) with a parameterization according

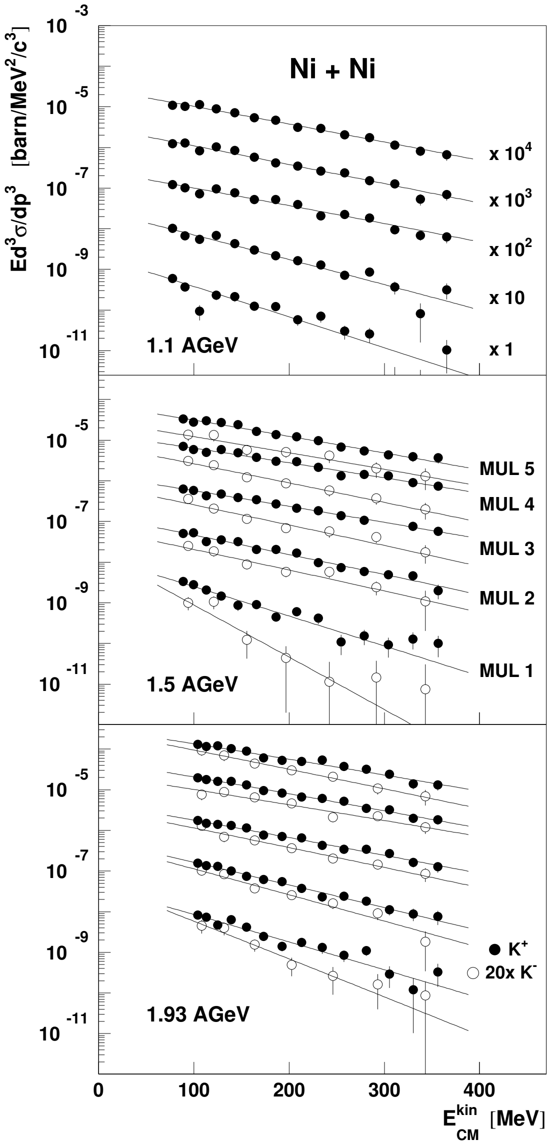

Fig. 1 *K^+ and K^- invariant cross sections as a function of the kinetic energy and the centrality of the reaction measured around midrapidity ($\theta_{lab} = 40° \pm 4°$) for Ni+Ni collisions at different beam energies (preliminary).*

to $M_K \propto A_{part}^{\alpha}$ (lines). The multiplicities for MUL 1 are not shown because the errors in integrating the cross sections are larger compared to the other bins. Within the uncertainties of A_{part} we get a common $\alpha = 1.62 \pm 0.21$ for K$^+$ and K$^-$ and for all beam energies. Values of α larger than unity indicate that the nucleons participate more than once in the kaon production.

Energy	MUL	$\frac{\sigma_{R,MUL}}{\sigma_R}$	$4\pi\frac{d\sigma_K}{d\Omega_{CM}}$ [mb]	T [MeV]
1.5 AGeV K^+	1	0.41	2.2 ± 0.2	55 ± 4
	2	0.23	4.5 ± 0.4	79 ± 6
	3	0.18	6.2 ± 0.5	96 ± 7
	4	0.14	7.2 ± 0.5	101 ± 8
	5	0.05	3.3 ± 0.3	93 ± 7
1.93 AGeV K^+	1	0.44	7.6 ± 0.7	58 ± 5
	2	0.23	14.8 ± 1.2	70 ± 6
	3	0.16	18.1 ± 1.4	88 ± 7
	4	0.11	21.4 ± 1.6	91 ± 7
	5	0.06	14.8 ± 1.2	97 ± 7
1.5 AGeV K^-	1	0.41	0.06 ± 0.011	33 ± 3
	2	0.23	0.10 ± 0.012	74 ± 6
	3	0.18	0.12 ± 0.013	78 ± 7
	4	0.14	0.13 ± 0.014	80 ± 7
	5	0.05	0.07 ± 0.011	90 ± 10
1.93 AGeV K^-	1	0.44	0.30 ± 0.06	43 ± 3
	2	0.23	0.51 ± 0.07	63 ± 7
	3	0.16	0.56 ± 0.06	79 ± 10
	4	0.11	0.57 ± 0.07	96 ± 8
	5	0.06	0.46 ± 0.05	81 ± 7

Table 1 *Relative reaction cross sections, K^+ and K^- production cross sections and inverse slope parameters as a function of the centrality for Ni+Ni collisions at beam energies of 1.5 and 1.93 AGeV (preliminary).*

In Figure 3 we present the K$^-$/K$^+$ ratio as a function of the impact parameter b for the beam energy 1.5 AGeV (full triangles) and 1.93 AGeV (full squares). Within the error bars the values are constant between 1.8 fm and 6 fm and the averaged ratios are 0.020 ± 0.004 for 1.5 AGeV and 0.031 ± 0.004 for 1.93 AGeV. The ratio for 1.93 AGeV agrees with the value of 0.031 ± 0.005 for non-central and near-central collisions in Ni+Ni measured for the full rapidity range ($\theta_{lab} = 28°$ to $64°$) at the same beam energy [3]. All measured K$^-$/K$^+$ ratios for Ni+Ni can be compared with the smaller system C+C [2] and the corresponding inclusive values of 0.025 ± 0.007 for the beam energy 1.8 AGeV and 0.038 ± 0.013 for 2.0 AGeV.
In conclusion, the K$^-$/K$^+$ ratio at a given bombarding energy is constant as a function of the centrality of the reaction and the size of the collision system. This observation is in agreement to the hypothesis, that the antikaon yiel d is coupled to the kaon yield via the strangeness exchange reaction $Y\pi \rightarrow K^-N$ (with $Y = \Lambda, \Sigma$).

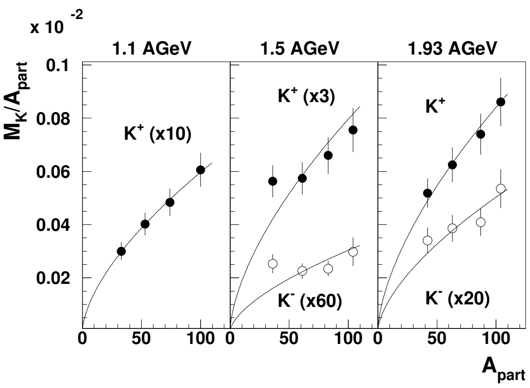

Fig. 2 *Kaon and antikaon multiplicity per A_{Part} as a function of A_{Part} for Ni+Ni collisions at beam energies of 1. 1, 1.5 and 1.93 AGeV (preliminary).*

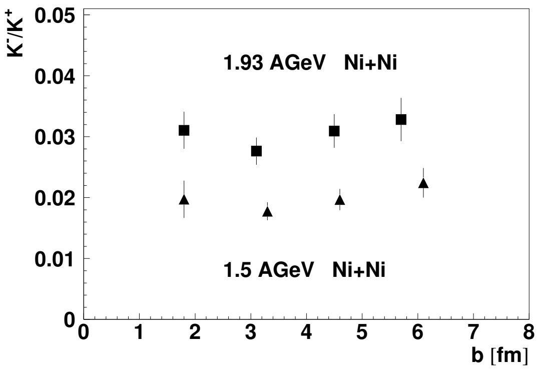

Fig. 3 *K^-/K^+ ratio as a function of the impact parameter b for Ni+Ni collisions at beam energies of 1.5 and 1.93 AGeV (preliminary).*

[1] *GSI Darmstadt* [2] *TU Darmstadt*
[3] *GSI Univ. Frankfurt* [4] *Univ. Marburg*
[5] *GSI Univ. Krakow* [6] *FZ Rossendorf*
[7] *TU Dresden* * *now at Ohio State Univ., Columbus, USA*

References

[1] R. Barth et al., Phys. Rev. Lett. 78 (1997) 4007
[2] F. Laue et al., Phys. Rev. Lett. 82 (1999) 1640
[3] M. Menzel et al., Phys. Lett. B 495 (2000) 26
[4] Y. Shin et al., Phys. Rev. Lett. 81 (1998) 1576

Comparison of First Results of K$^+$ Production at ANKE with Model Calculations [B]

Ch. Schneider, H. Müller and ANKE Collaboration

Kaon production in the reaction p+C→K$^+$+X has been measured with the ANKE spectrometer [1] at beam energies of 2.3, 1.8, 1.5, 1.2 and 1.0 GeV. The calibration of the data is still in progress, nevertheless the detected and analysed Kaon rates can be compared with the ROC-model [2] calculations if the acceptance and efficiency of the detection process at ANKE is taken into account. Thus the ROC-model was used as a data generator for GEANT simulations of the ANKE side detector system.

In Fig. 1 the detection efficiencies for Kaons from such simulations are shown. They are plotted as a function of the telescope number, normalised to the total number of Kaons. Curve **b** shows the number of Kaons generated in the acceptance range of each considered telescope. The difference to the curve **a** represents the losses due to scattering and due to the gaps between the telescopes. Curve **c** takes into account the loss due to cuts on time of flight and energy loss in the scintillation counters. Curve **d** takes the lifetime of the Kaons on their way through the detector into acount. Curve **e** shows the finally counted particles in the veto counter with a decay time larger than 2.6 ns.

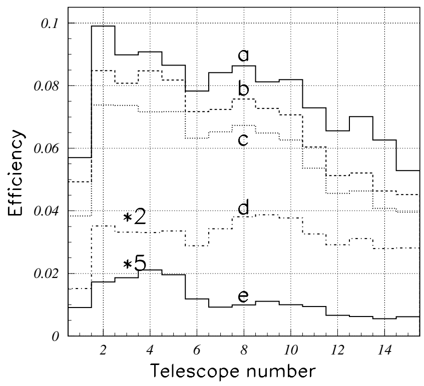

Fig. 1 *Simulation of K$^+$ verification with the ANKE side detector system as a function of telescope number. The curves are explained in the text.*

Very primilary results of the data analysis for beam energies of 1.0 GeV and 1.2 GeV are shown in Fig. 2. The raw numbers of extracted Kaons for the specified data collecting time are plotted as a function of the mean particle momentum measured in every telescope. A peliminiary normalisation to comparable experiment conditions results in a factor of ∼ 30 [3] between the cross sections at the two energies. The cross sections obtained from the ROC-Geant simulations are plotted in Fig. 3. They take into account all losses described in Fig. 1. The ratio of the measured production rate at 1.0 GeV and 1.2 GeV at the covered forward angle around 0° is comparable to the prediction of our simulation.

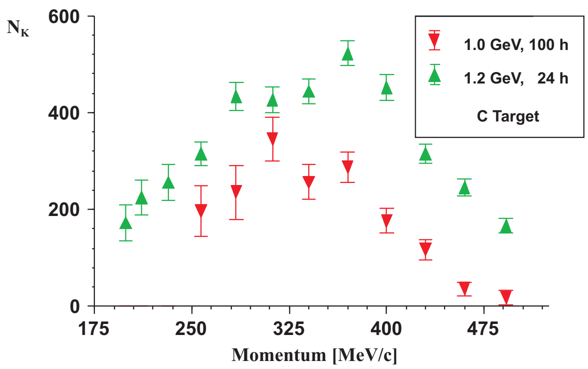

Fig. 2 *Number of indetified Kaons in each telescope from the experimental runs at 1.2 and 1.0 GeV [1]*

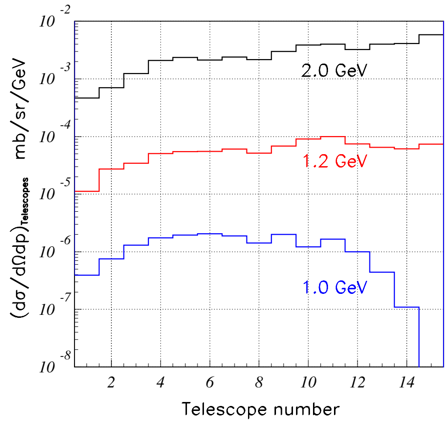

Fig. 3 *Simulated detection cross sections, when the ROC-model is used as a generator for GEANT simulation of the ANKE spectrometer*

References

[1] S. Barsov et al., Nucl. Phys. A 675, 230 (2000)
[2] H. Müller, Z. Phys. A 355, 223 (1996)
[3] M. Büscher et al., publication in preparation

Investigation of the Associated Strangeness Production in the Reaction $pp \to pK^+\Lambda$ [B,K]

K. Möller, S. Dshemuchadse

One of the main topics of the physics program of the COSY TOF collaboration is the investigation of the associated strangeness production in pp reactions at COSY energies up to 2.5 GeV. Quite a lot of data has been accumulated in recent beam times. So, there is an urgent need for analysing these data. To support and speed up the analysis a computer code was developed by the Rossendorf COSY TOF group for analysing the associated strangeness production of Λ hyperons. In this code a new concept was applied to search for primary and secondary tracks in the data.

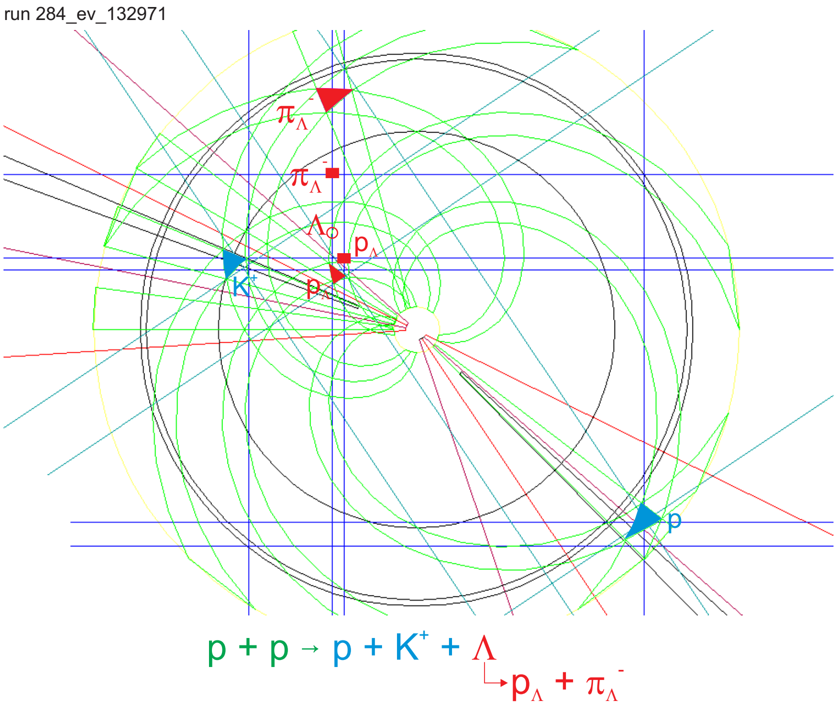

Fig. 1 *A $pK\Lambda$ event at proton momentum 2.85 GeV/c.*

One example is shown in Fig. 1 which demonstrates that the developed computer code is capable of detecting pKΛ events. In the figure a hit display is shown with the following colour assignments for the different position sensitive detector elements: start detector sectors (red), microstrip sector and ring elements (black), fiber hodoscope 1 (blue), fiber hodoscope 2 (blue-green) and the endcap (quirl) elements (green). In the first step of the pp-reaction shown in Fig. 1 a proton, a kaon and a lambda particle are generated with the latter one decaying into a proton and a pion in a secondary process. After the software development was finished in a first check a data tape was reanalysed which was analysed somewhat earlier by the Erlangen COSY TOF group. In most cases good agreement was found in the set of event numbers attributed to $pK\Lambda$ events. For events with event numbers which did not coincide the reason for the disagreement was analysed. This led to a further refinement of the computer codes. Thus by applying two different codes for data analysis the accuracy of the results obtained by the TOF collaboration can be significantly increased. After checking the reliability of the Rossendorf $pK\Lambda$ analysis concept the developed computer code is now ready to be applied to data not yet analyzed up to now. Due to the modular structure of the analysis program (written in C++) the code can easily be modified to analyse also channels other than the associated Λ production, e.g., the Σ production in the channels $pp \to pK^+\Sigma^0$ and $pp \to pK^0\Sigma^+$.

Strangeness in Quark Stars [B]

A. Peshier[1], B. Kämpfer, G. Soff[2]

There is the long standing conjecture that in the cores of neutron stars the matter resides in a deconfined state (cf. [1] and further references therein). Basing on the speculation of self-bound strange quark matter also pure strange quark stars have been predicted (cf. [2] for a reference list for this topic). The theoretical study of this subject was hampered up to now by the poorly known equation of state at large baryon density. However, recently a considerable progress has been made in calculating the equation of state at vanishing baryon density [3].

In [4] we have shown that the lattice QCD data can be described within a quasiparticle model. This model allows to map the lattice results to finite baryon density. Provided the quasiparticle nature does not change, the equation of state is accessible in such a way. Surprisingly, the numerically obtained results at vanishing temperature can be approximated by $p = \alpha e - 4\tilde{B}$, where p is the thermodynamical pressure, e the total energy density, $\alpha = 3.0 \cdots 4.5$ and $\tilde{B}^{1/4} = 200 \cdots 260$ MeV. The ranges of α and $\tilde{B}$ are a direct consequence of the yet existing uncertainty of the lattice QCD results.

Exploiting the given parameterization one can integrate the TOV equations to get the masses and radii of cold, pure quark stars in local β equilibrium, as displayed in Figs. 1 and 2. Due to the β equilibrium a large fraction of the quarks occurs as strange quarks.

Of course, the existence of pressure-free deconfined matter is questionable, therefore, one should study hybrid stars by *interpolating* from our high-density equation of state to nuclear matter densities, where the equation of state is fairly well known.

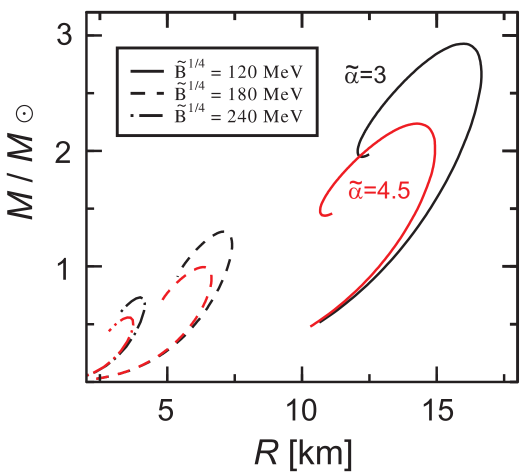

Fig. 1 *The dependence of the mass of pure quark stars with strangeness on the radius for several values of the parameters* α *and* $\tilde{B}^{1/4}$.

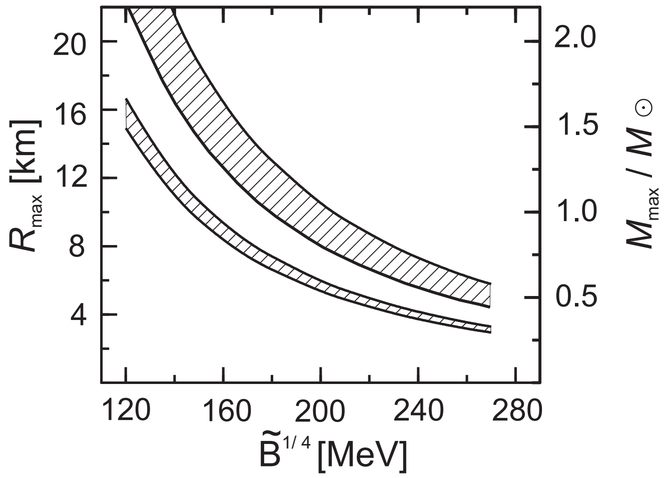

Fig. 2 *Maximum masses (upper hatched band, right scale) and corresponding radii (lower hatched band, left scale) of pure quark stars as a function of* $\tilde{B}^{1/4}$. *The upper (lower) limit of the bands is for* $\alpha = 3$ *(4.5).*

[1] *Dept. of Physics, Brookhaven Nat. Lab., Upton, NY 11973, USA*
[2] *Institut für Theoretische Physik, TU Dresden*

References

[1] B. Kämpfer, J. Phys. A 14 (1981) L471, Phys. Lett. B 158 (1984) 121
[2] K. Schertler, C. Greiner, J. Schaffner-Bielich, M.H. Thoma, Nucl. Phys. A 677 (2000) 463
[3] F. Karsch, E. Laermann, A. Peikert, Phys. Lett. B 478 (2000) 447
[4] A. Peshier, B. Kämpfer, G. Soff, Phys. Rev. C 61 (2000) 045203

Electroproduction of Kaons and Light Hypernuclei [B,W]

F. Dohrmann[1,2] for the Jefferson Laboratory Experiment E91-016 collaboration

Jefferson Laboratory experiment E91-016, "Electroproduction of Kaons and Light Hypernuclei" is a study of quasifree production of Kaons on targets of H, D, ^{3}He, ^{4}He, Carbon and Aluminum, at an incident electron energy of 3.245 GeV. For H and D targets, data were also obtained at E = 2.445 GeV. The scattered electron e' and emergent K^+ were detected in coincidence with the use of the HMS and SOS spectrometers, respectively, in Hall C of Jefferson Laboratory. Angular distributions for the (e,e'K^+)Y reactions were measured at forward angles with respect to the virtual photon for $Q^2 \simeq 0.35\,\mathrm{GeV}^2$. Particle identification utilizing time-of-flight detectors together with Aerogel Cerenkov detectors yields clean missing mass spectra [1], and allows subtraction of random backgrounds. The experiment was run in two time periods. The H and D targets were studied near the end of 1996 while the balance of the experiment, namely the $^{3,4}He$ targets were bombarded in the fall of 1999 when the FZR also collaborated on running the experiment. More than 1.4 TB of data were taken during that time.
The fundamental interaction being studied is N(e,e'K^+)Y where Y is either a Λ or Σ and N represents a nucleon. For the H target, the final state can only be a Λ or Σ, but for heavier targets, there is relative motion between the nucleons in the target that results in broadening of the peaks. For the D target, it is possible to separate the two peaks inasmuch as the Fermi broadening is not large compared to the mass difference [2]. For ^{3}He and ^{4}He, very preliminary missing mass spectra being shown in Fig 1, it will be more difficult to separate the yields for the various final states. Even in this early stage of analysis, it is quite clear that the width of the quasifree peak is greater in ^{4}He (more binding) than in ^{3}He.

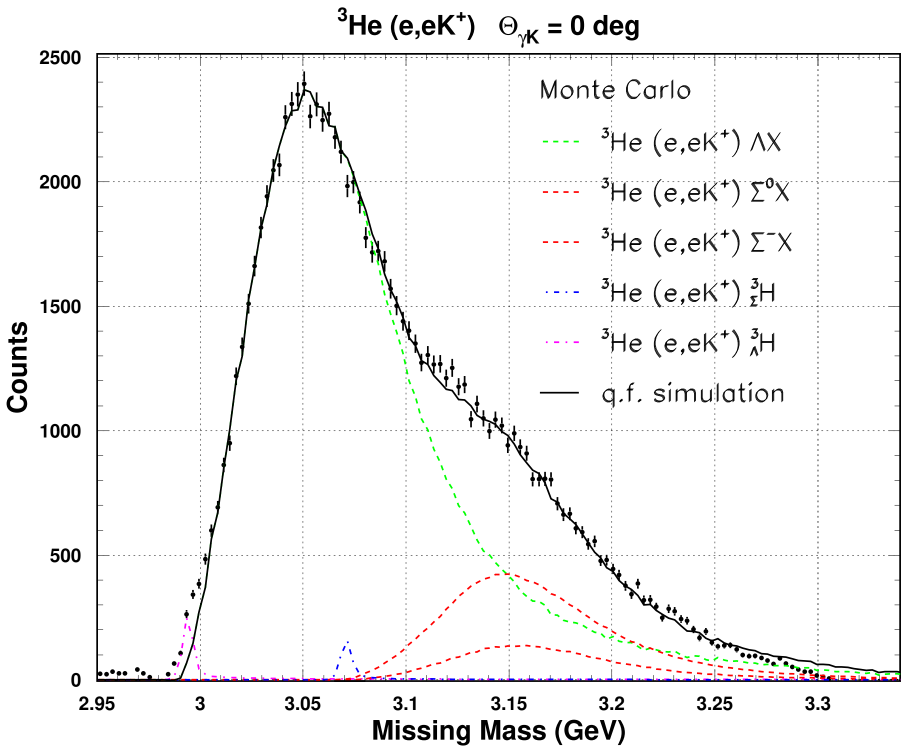

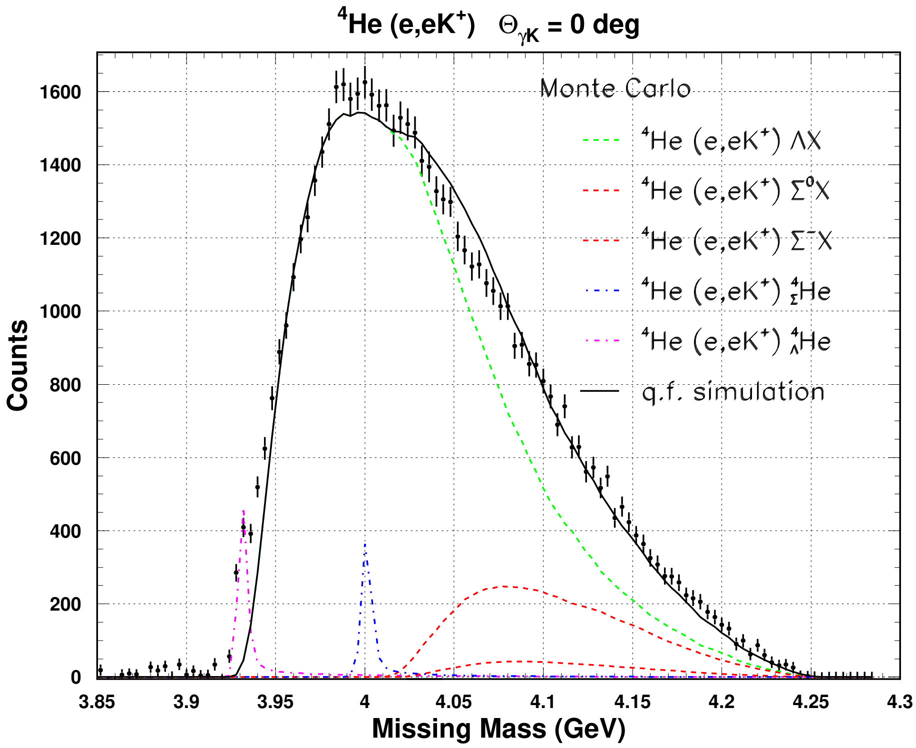

Fig. 1 *Preliminary missing mass spectra for* ^{3}He *and* $^4\mathrm{He(e,e'K^+)}$ *reactions for a relative angle of* 0 deg *in the lab between the virtual photon and the Kaon. The various Monte-Carlo simulations for the quasi-free contributions as well as their sum (solid line) are shown. They are preliminary and relatively crude. The location of "bound* Λ *and* Σ*" states is shown merely to suggest possible locations. It should be emphasized that much more analysis is required.*

For D, it is known that there is no bound Λ-nucleon state, but for both ^{3}He and ^{4}He targets we anticipate evidence for a bound hypernuclear states. Although the data shown in the figure are quite preliminary, it appears that bound Λ hypernuclear states are seen. The possibility of bound Σ hyper-nuclei also exists, but it is conjectural at this time. Construction of an optimal Monte-Carlo simulation will require considerably more effort before any conclusions can be drawn. The large number of final state configurations results in complications that must be analyzed prior to extracting final cross sections.
Together with Carbon and Aluminum the complete data set contains five different targets and provides a high-statistics study of the mass dependence of Kaon electroproduction on light nuclei.

[1] *FZR and Physics Division, Argonne National Laboratory, Argonne, Illinois 60439, USA*
[2] *presently Feodor Lynen Research Fellow at Argonne National Laboratory, Argonne, Illinois 60439, USA*

References

[1] ANL Annual Report # ANL99-12, Fig. III-6
[2] D. Abbott et al., Nucl. Phys. A 639 (1998) 205c

Production of ϕ Mesons in Near-Threshold πN and $N N$ Reactions [B,W]

A.I. Titov[1], B. Kämpfer, B.L. Reznik[2]

In previous work [1] we have demonstrated that various observables in the reactions $NN \to \phi NN$ and $\pi N \to \phi N$ show some sensitivity to an admixture of hidden strangeness in the nucleon. It turns out, however, that, within the extended one-boson-exchange model, the effective coupling constants and cut-off parameters are poorly constrained. We have, therefore, continued our analysis to explore the ϕ production mechanism within a conventional one-boson-exchange model by including the recent results of the DISTO collaboration. Our calculated cross sections are displayed in Figs. 1 and 2 together with experimental data.

The data and other constraints of the model parameters are still insufficient to derive a unique set of parameters. Rather there is a wide range of the commonly used cut-off parameter $\Lambda_{\phi\rho\pi}$ entering the $\phi\rho\pi$ vertex. Some observables, such as the total cross section as a function of the excess energy and the angular distribution, are less sensitive to variations of $\Lambda_{\phi\rho\pi}$. Polarization observables and observables related to the subsequent decays $\phi \to e^+e^-$ and $\phi \to K^+K^-$ can serve as further constraints to the parameter space.

A detailed understanding of the ϕ production dynamics, in particular the cross sections at small excess energies, is a necessary prerequisite for a profound analysis of the kaon and dilepton channels in heavy-ion collisions.

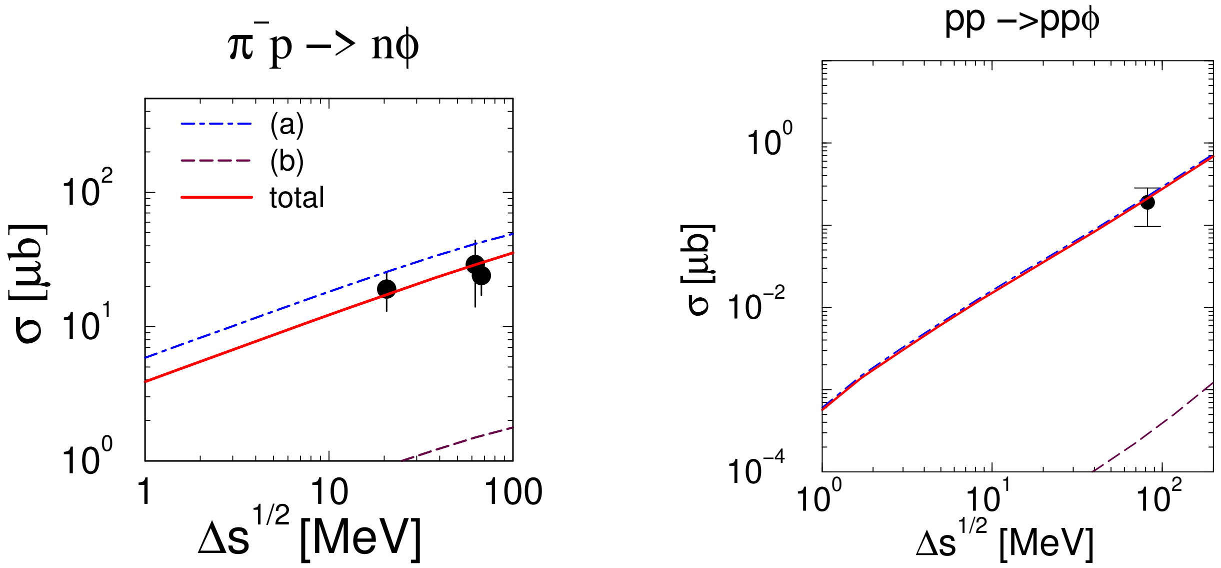

Fig. 1 *The calculated cross sections for the reactions $\pi^- p \to \phi n$ (left panel, data from [3]) and $pp \to \phi pp$ (right panel, data from [4]) as a function of the excess energy above the threshold. Dot-dashed curves: contribution from diagrams with a $\phi\rho\pi$ vertex, dashed curves: contributions from diagrams with direct ϕNN coupling, solid curves: resulting cross sections including interferences. Final state interaction has been included within the Jost function and phase-equivalent potential formalism. For further details see [2].*

[1] *Bogolyubov Laboratory of Theoretical Physics, JINR Dubna, Russia*
[2] *Far-Eastern State University, Vladivostok, Russia*

References

[1] A.I. Titov, B. Kämpfer, V.V. Shkyar, Phys. Rev. C 59 (1999) 999
[2] A.I. Titov, B. Kämpfer, B.L. Reznik, Eur. Phys. J. A 7 (2000) 543
[3] A. Baldini et al., Total cross sections of high energy particles, Springer-Verlag, Heidelberg, 1988
[4] F. Balestra et al. (DISTO Collaboration), Phys. Lett. B 468 (1999) 7

Sub-Threshold $\phi(1020)$ Meson Production in the Reactions Ni(1.93A·GeV)+Ni and Ru(1.69A·GeV)+Ru [B]

R. Kotte and the FOPI collaboration

First results on systematic investigations of sub-threshold ϕ meson production in heavy-ion reactions measured with the 4π detector system FOPI at GSI have been previously reported [1,2]. About $N_{ev} = 4.7 \cdot 10^6$ $(6.8 \cdot 10^6)$ central events comprising about 9% (15%) of the total cross section have been analysed for the system Ni+Ni (Ru+Ru) at 1.93 (1.69) A·GeV. We select candidates of charged kaons measured with the subdetectors Helitron (Hel) and outer Plastic Wall (Pla) within the polar angle and velocity acceptance limits of $\Delta\theta_K$ $(15^o < \theta < 27^o)$ and $\Delta\beta_K$ $(0.4 < \beta < 0.85)$, respectively. These limits confine a phase space sector located near the region of highest intensity, i.e. at mid-rapidity ($\beta_{cm} \sim 0.7$) and at low transverse momentum [1]. The efficiency-corrected ϕ multiplicity is determined via $P_\phi(\Delta\theta_K, \Delta\beta_K) = \frac{N_\phi(\Delta\beta_K,\Delta\theta_K)}{N_{ev}\cdot\epsilon^2_{det,K}(\Delta\beta_K,\Delta\theta_K)}$ with $N_\phi(\Delta\beta_K, \Delta\theta_K)$ being the number of ϕ's reconstructed from their decay kaons and $\epsilon_{det,K}(\Delta\beta_K, \Delta\theta_K)$ representing the kaon detection efficiency (incorporating the matching efficiency of Hel tracks with Pla hits and the cut efficiency of kaon selection). The efficiency is taken from pseudo kaons, i.e. protons of similar angular and momentum range as kaons [1]. (This method does not work for the FOPI subdetectors CDC and Plastic Barrel, since the latter one alone does not allow for particle identification. There, all efficiencies are included in the ϕ acceptance factor which is determined with the GEANT package simulating the detector response [2]. Since the acceptance depends strongly on the ϕ phase space distribution which is generated as input, e.g. by using a thermal model with temperature T, any ϕ yield extrapolated to 4π would depend on these assumptions, i.e. it would be model dependent.) For the Ni+Ni (Ru+Ru) system, the deduced ϕ multiplicity per central event in the Hel/Pla acceptance given by $\Delta\beta_K$ and $\Delta\theta_K$ amounts to $P_\phi(\Delta\theta_K, \Delta\beta_K) \cdot 10^5 = 4.8 \pm 2.0$ (3.1 ± 1.2).

These numbers can be compared directly with the output of transport approaches when implementing the detector acceptance/geometry and the decay properties of both the ϕ mesons and the daughter kaons. Appropriate transport model calculations have been performed recently [3]. Extending the IQMD transport model to ϕ meson production a total of $3.5 \cdot 10^{-4}$ $(2.2 \cdot 10^{-4})$ ϕ mesons per central event has been calculated for the Ni+Ni (Ru+Ru) system. Filtering the decay kaons through the acceptance limits described by $\Delta\beta_K$ and $\Delta\theta_K$ and taking into account the branching ratio of the decay $\phi \to K^+K^-$ of 49.1% and the finite kaon lifetime ($c\tau = 3.71$ m) a ϕ yield of $1.8 \cdot 10^{-6}$ $(1.1 \cdot 10^{-6})$ is found for the Ni+Ni (Ru+Ru) system.

The ratio of the yields with/w.o. filtering gives a typical ϕ acceptance of 0.5%. Since the total ϕ rapidity and transverse momentum spectra of the transport approach can be well approximated by an isotropic thermal distribution with $T = 60 - 70$ MeV, quite similar acceptance factors (including the $\phi \to K^+K^-$ branching) are calculated also within our Monte-Carlo simulations when adopting this effective temperature [1].

For both considered systems, the ϕ yield predicted by the transport model is substantially smaller than the experimental values. Also, an earlier attempt to predict the ϕ production in the Ni+Ni reaction within the framework of another transport approach [4] delivered deviations of similar size though the involved elementary cross sections (esp. $pp \to pp\phi$) are quite different. The reason for this strong underestimation of ϕ meson production in both central heavy-ion reactions investigated at beam energies below the nucleon-nucleon threshold (2.54 A·GeV) is not yet understood. Therefore, further theoretical work is advisable [5].

References

[1] R. Kotte (FOPI collaboration), Proc. Int. Workshop XXVIII, Hirschegg, Austria, Jan. 2000, p. 112
[2] N. Herrmann (FOPI collaboration), Nucl. Phys. A 610 (1996) 49c
[3] C. Hartnack and J. Aichelin, private communication
[4] W.S. Chung, G.Q. Li, and C.M. Ko, Nucl. Phys. A 625 (1997) 347
[5] H.W. Barz, B. Kämpfer, G. Wolf, and M. Zétényi, this Report

The Role of Three-Body Collisions in ϕ Meson Production Processes Near Threshold [B]

H.W. Barz, B. Kämpfer

Currently there is much interest in subthreshold production of heavy mesons in relativistic nuclear collisions. It is expected that measurements will reveal the change of the properties of mesons in dense and hot nuclear matter. Recent measurements [1] of ϕ mesons in Ni+Ni and Ru+Ru collisions point to relatively large production cross-sections which could not be understood till now within the framework of transport models [2].
Therefore, we study whether three-body collisions could remarkably contribute to the production of ϕ mesons in heavy-ion collisions. Such processes have the advantage that three nucleons can share their energy. The cross section for the reaction N+2N $\to \phi$ + 3N is calculated using tree-level diagrams indicated in Fig. 1. If the momentum of an intermediate particle (ρ, π, B) in a diagram gets on shell its value becomes singular and the diagram describes two consecutive two-body processes. Such two-step processes are usually considered in the transport models. Therefore, we have defined the genuine tree-body process after separating the singular parts from the diagrams. The upper line in Fig. 2 shows the cross section for this genuine process. However, if absorption processes in the medium are included this cross section is strongly diminished and can even take a negative value. The two-step processes with intermediate π and ρ mesons give together a larger cross section than that calculated with the three-body diagrams, see Fig. 2.
We conclude that genuine three-body processes are not important in nuclear matter as most of the strength can be evaluated via consecutive two-body reactions. In the case considered here the two-step processes slightly overestimate the cross section. However, it is necessary that all intermediate particles which can reach the energy shell are treated properly within transport-model calculations as they essentially contribute to particle production.

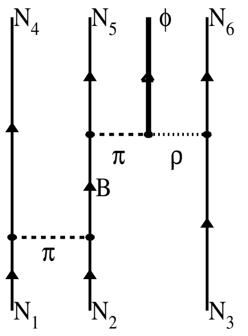

Fig. 1 *Topology of tree-level diagrams contributing to the three-body ϕ meson production. Further diagrams are used arising from time reordering and particle exchanges.*

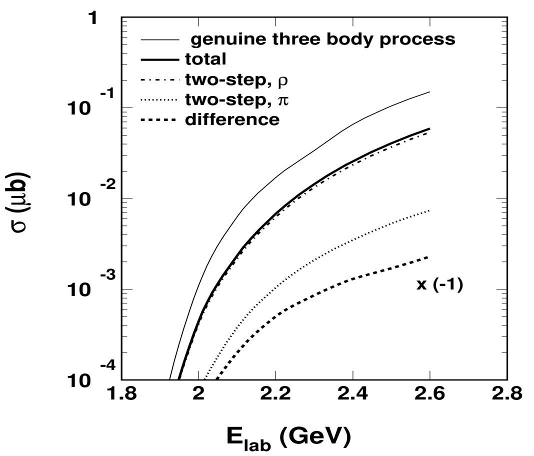

Fig. 2 *Cross section of ϕ meson production by a proton hitting a proton in a proton environment. The thin line gives the three-body cross section without intermediate rescattering whereas the other lines show the results with rescattering. For further details consult [3].*

References

[1] R. Kotte (FOPI collaboration), Proc. Int. Workshop XXVIII, Hirschegg, Austria, 2000, p. 112

[2] W.S. Chung, G.Q. Li and C.M. Ko, Nucl. Phys. A 625 (1997) 347

[3] H.W. Barz and B. Kämpfer, Nucl. Phys. A 683 (2001) 594

Cross Sections for ϕ Meson Production in ρ Meson–Baryon Collisions [B,A]

H.W. Barz, M. Zétényi[1]

Recently ϕ meson production was measured in subthreshold Ni+Ni and Ru+Ru collisions by the FOPI collaboration at the heavy-ion synchrotron at GSI Darmstadt [1]. The ϕ meson yield found in these experiments is considerably larger than the predictions of Boltzmann-Ühling-Uhlenbeck (BUU) calculations [2]. A possible explanation could be the existence of new ϕ production channels that have not been considered so far in BUU calculations. Therefore, we study the ϕ production cross sections in ρ-N and ρ-Δ collisions.

We calculate the isospin averaged cross sections in a one-boson exchange model. In this case a single pion exchange diagram contributes to both processes. The differential cross section can be written as

$$\frac{d\sigma}{d\Omega} = \frac{1}{64\pi^2 s}\frac{|\mathbf{p}_{out,CM}|}{|\mathbf{p}_{in,CM}|}|\mathcal{M}|^2. \tag{6}$$

The quantity $|\mathcal{M}|^2$ represents the squared matrix elements summed over the final and averaged over the initial spin and isospin states. These expressions read for the ρ-N channel

$$|\mathcal{M}|^2 = 32\left(\frac{A_{\rho N\to\phi N}}{p_\pi^2 - m_\pi^2}\right)^2 m_N^2\left(p_N\cdot p_{N'} - m_N^2\right)\left((p_\rho\cdot p_\phi)^2 - m_\rho^2 m_\phi^2\right) \tag{7}$$

and for the ρ-Δ channel

$$|\mathcal{M}|^2 = \frac{16}{9}\left(\frac{A_{\rho\Delta\to\phi N}}{p_\pi^2 - m_\pi^2}\right)^2 (p_\Delta\cdot p_N + m_\Delta m_N)\left((\frac{p_\Delta\cdot p_N}{m_\Delta})^2 - m_N^2\right)\left((p_\rho\cdot p_\phi)^2 - m_\rho^2 m_\phi^2\right). \tag{8}$$

Here, the incoming four-momenta are denoted by p_ρ, p_Δ and p'_N while the p_N and p_ϕ are the outgoing momenta. The factors A_i are given by $A_{\rho N\to\phi N} = (f_{\pi NN}f_{\pi\rho\phi}/m_\pi m_\phi)F_{\pi NN}(p_\pi^2)F_{\pi\rho\phi}(p_\pi^2)$ and $A_{\rho\Delta\to\phi N} = (f_{\pi N\Delta}f_{\pi\rho\phi}/m_\pi m_\phi)F_{\pi N\Delta}(p_\pi^2)F_{\pi\rho\phi}(p_\pi^2)$. Substituting the appropriate values for the coupling constants f_i and the cutoff parameters appearing in the form factors $F_i(p_\pi^2)$ and integrating Eq. (1) numerically over the angle we obtain the total cross sections. Their values are displayed in Fig. 1 as a function of the CM energy above threshold using the peak masses of the resonance states involved. For comparison we have included the cross section for the process $\pi + N \to N + \phi$ [2]. The obtained cross sections for ϕ meson production in ρ channels are much higher than that of the π-N channel, therefore the ρ-baryon channels can essentially contribute to ϕ production in heavy-ion collisions despite their relative small abundances.

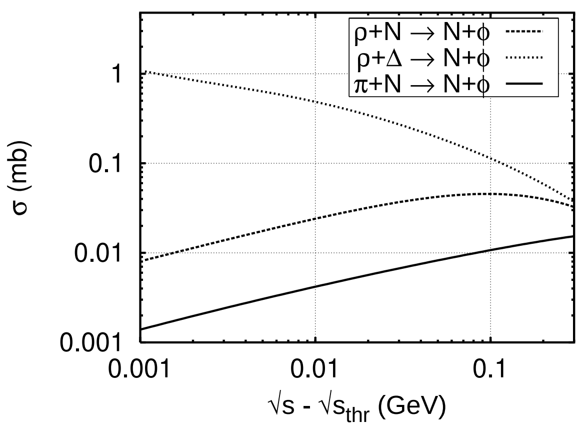

Fig. 1 *Total cross section of ϕ meson production in the reactions $\rho + N \to N + \phi$ and $\rho + \Delta \to N + \phi$. For comparison the cross section for the process $\pi + N \to N + \phi$ is also included. Note that the threshold for the $\rho+\Delta$ process lies in the incoming channel.*

[1] *KFKI Budapest, Research Institute for Particle and Nuclear Physics, H-1525 Budapest, POB 49, Hungary*

References

[1] R. Kotte (FOPI collaboration), Proc. Int. Workshop XXVIII, Hirschegg, Austria, 2000, p. 112
[2] W.S. Chung, G.Q. Li and C.M. Ko, Nucl. Phys. A 625 (1997) 347

Influence of ρ Meson Channels on ϕ Meson Production in Heavy-Ion Collisions [B,A]

H.W. Barz, B. Kämpfer, Gy. Wolf[1], M. Zétényi[1]

The study of meson production in heavy-ion collisions near threshold gives insight in the particle properties in dense matter. Furthermore information on the equation of state is provided as the particle production rates depend sensitively on the potentials the collision partners feel. Recently, the ϕ meson production was measured in reactions of Ni+Ni and Ru + Ru at energies of 1.93 and 1.69 A·GeV, respectively [1]. Extrapolations from the limited phase space available point to a larger cross section than standard Boltzmann-Ühling-Uhlenbeck (BUU) calculations [2]. These calculations usually do not consider the production of ϕ mesons by elementary collisions of ρ mesons and baryons. The cross sections of these reactions are larger than those of pions. To study the influence of these channels a version of the BUU code [3] was used which explicitly treated ρ mesons created in pion-pion collisions or in resonance decays. This version was applied to central collisions of Ru+Ru with an impact parameter smaller than 4.2 fm. We found that $2 \cdot 10^{-3}$ ϕ mesons are produced per event and roughly 2/3 of them stem from ρ-N and ρ-Δ collisions. In Fig. 1 we show the transverse mass spectrum at midrapidity from which an effective temperature of $T = 85$ MeV is deduced. Taking into account the detector acceptance of the FOPI apparatus [1] the expected ϕ meson distribution in the rapidity-transverse momentum plane is shown in Fig. 2, altogether there are $0.8 \cdot 10^{-5}$ particles per central event. This number is still by about a factor of four smaller than the experimental value of $(3.1 \pm 1.2) \cdot 10^{-5}$ [4].

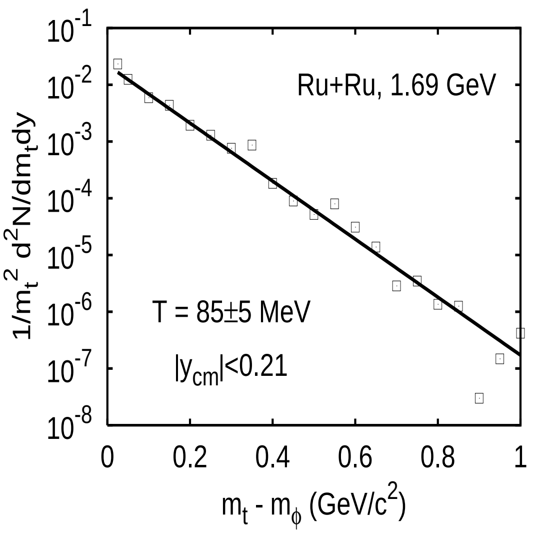

Fig. 1 *Calculated transverse mass spectrum (open squares) of ϕ mesons at midrapidity. The solid line shows the fit to the Boltzmann distribution $exp(-m_t/T)$.*

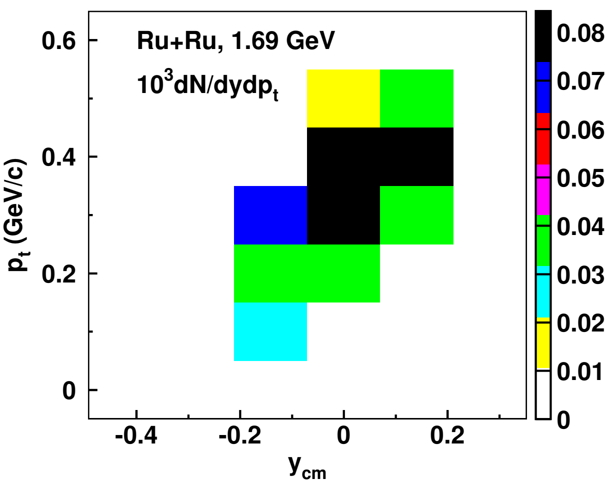

Fig. 2 *Calculated distribution of $dN/dydp_t$ of ϕ mesons per event in the rapidity - transverse momentum plane taking the FOPI detector acceptance into account.*

[1] *KFKI Research Institute for Particle and Nuclear Physics, H-1525 Budapest, POB 49, Hungary*

References

[1] R. Kotte (FOPI collaboration), Proc. Int. Workshop XXVIII, Hirschegg, Austria, Jan. 2000, p. 112
[2] W.S. Chung, G.Q. Li and C.M. Ko, Nucl. Phys. A 625 (1997) 347
[3] Gy. Wolf, W. Cassing, U. Mosel, Nucl. Phys. A 552 (1993) 549
[4] R. Kotte, this Report

Production of ω Mesons in pp Collisions at Q = 89 MeV

R. Dressler, I. Fröhlich[1], E. Grosse, W. Kühn[1], H.-W. Pfaff[1], J. Ritman[1]
for the DISTO collaboration

In the course of the experiments with the two-arm DISTO [1] spectrometer at the SATURNE accelerator in Saclay the exclusive production of ω mesons was measured at excess energies Q = 89, 207, and 320 MeV ($Q = \sqrt{s} - \sqrt{s_0}$). These beam energies are well suitable to close the considerable gap between the near-threshold data obtained in SPEC III experiments [2] at excess energies Q < 30 MeV and data at larger Q > 400 MeV (see e.g. [3]).
Data at the highest beam energy in DISTO experiments were analyzed and published so far [4-7]. The investigation of all data is still in progress. In this contribution first preliminary results on the analysis of the data at the lowest excitation energy for the ω meson are presented.
The exclusive reactions pp$\rightarrow$ppη and pp$\rightarrow$ppω were identified via the three pion decay (i.e. $\eta, \omega \rightarrow \pi^+\pi^-\pi^0$), where the braching ratios are taken from [8]. Only events with one negative and three positive charged particles were used in the data processing of η and ω mesons. A good separation was achieved for π^+ and p, also the π^- was clearly observed as shown in [4-6] using the light signal from the water filled Cerenkov detectors together with the particle momentum. Fig. 1 shows the $(M_{\rm inv}^{pp\pi^+})^2 - (M_{\rm miss}^{\pi^-})^2$ distribution, whereas the symbol $(M_{\rm inv/miss}^{x})$ denotes the invariant or the missing mass of the particle or particle combination x. In Monte Carlo simulations only the region above 0.4 (GeV/c^2)^2 was populated with η and ω mesons. Therefore, this behavior was used to suppress pure 4 body events (pp$\pi^+\pi^-$) in the data analysis, which are peaked at $(M_{\rm inv}^{pp\pi^+})^2 - (M_{\rm miss}^{\pi^-})^2 = 0$ (GeV/c^2)^2.
To improve the resolution of the $(M_{\rm miss}^{pp\pi^+\pi^-})^2$ spectrum a kinematical refit assuming a missing π^0 meson was applied in a second fit procedure. The spectrum after this refit is shown in Fig. 2. The arrows depict the expected positions for the mesons taken from [8]. The main source of the remaining background is the non-resonant $\pi^+\pi^-\pi^0$ production. Unfortunately, the exact form of the background is unknown. Therefore, the spectrum was fit with Gauss peaks for the η and ω signals and the background was parametrized with a polynomial of third order and a wide Gaussian curve. In Fig. 2 are also depicted the fit result (full), the η and ω peak (dashed), and the background (dotted), respectively.

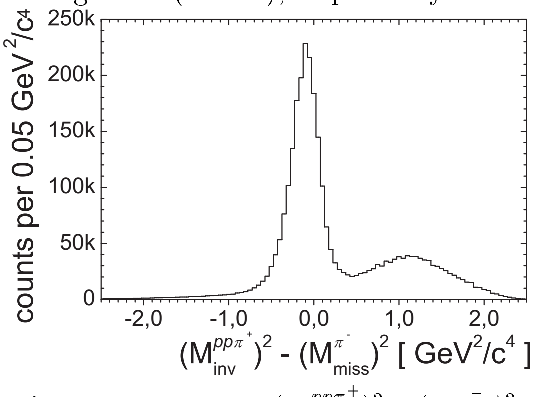

Fig. 1 *Distribution of* $(M_{\rm inv}^{pp\pi^+})^2 - (M_{\rm miss}^{\pi^-})^2$.

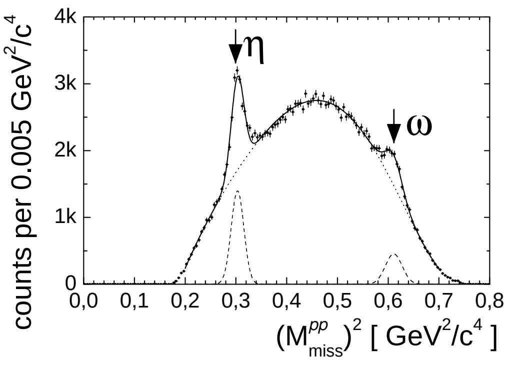

Fig. 2 $(M_{\rm miss}^{pp})^2$ *spectrum after kinematic refit.*

[1] *II. Physikalisches Institut, Justus-Liebig-Universität Gießen*

References

[1] F. Balestra et al., Nucl. Instr. Meth. A 426, 385 (1999)
[2] F. Hibou et al., Phys. Rev. Lett. 83, 492 (1999)
[3] R. Baldi et al., Phys. Lett. B 68 (1977) 381
[4] F. Balestra et al., Phys. Rev. Lett. 81, 4572 (1998)
[5] F. Balestra et al., Phys. Lett. B 468, 7 (1999)
[6] F. Balestra et al., Phys. Lett. B 491, 29-35 (2000)
[7] F. Balestra et al., Phys. Rev. C 63, 024004 (2001)
[8] D.E. Groom et al., Eur. Phys. J. C 15, 1 (2000)

Production of a_0^+ Mesons in the Reaction $pp \to da_0^+$ [B]

H. Müller

The structure of the lightest scalar mesons $a_0(980)$ and $f_0(980)$ is not well understood (see the “note on scalar mesons” of the particle data group [1]). In a recent paper [2] the necessity of new measurements of a_0 production and of a_0 branching ratios for clarifying the a_0 structure has been emphasized. Such an experiment is presently prepared at COSY [3].

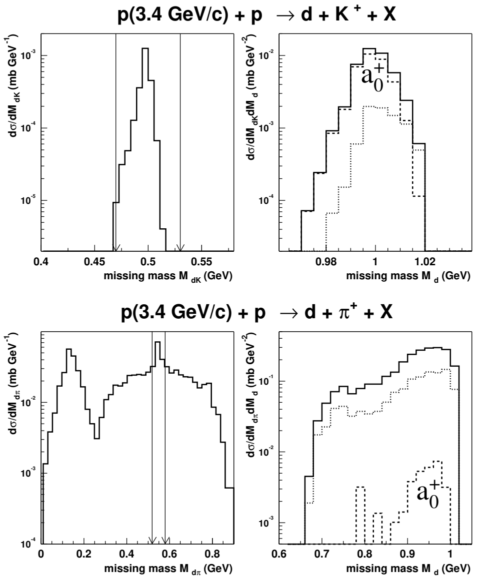

Fig. 1 *Missing mass distributions for the reactions $pp \to dK^+X$ (upper panels) and $pp \to d\pi^+X$ (lower panels) calculated at incidence momentum* 3.4 GeV/c *for polar angles $\Theta \leq 10°$ and 1.5% momentum resolution. The two arrows in the left hand panels indicate the windows in the M_{dK} and $M_{d\pi}$ distributions, which are used in the calculation of the M_d distribution shown in the right hand panels. The dashed histograms indicate the contributions from the reaction $pp \to da_0^+$, the dotted histograms those of the nonresonant channels $pp \to dK^+\bar{K}^0$ and $pp \to d\pi^+\eta$, respectively.*

Although in Ref. [2] predictions for the reaction $pp \to da_0^+$ at COSY energies have been given, no attempt has been made to compare the channels with a_0^+ production and subsequent decays, $pp \to da_0^+ \to dK^+\bar{K}^0$ and $pp \to da_0^+ \to d\pi^+\eta$, with the nonresonant channels $pp \to dK^+\bar{K}^0$ and $pp \to d\pi^+\eta$. For the measurement of a_0^+ production the latter channels might be rather disturbing if they are of high intensity. Another source of background are multipion channels, where two or three pions may have an invariant mass similar to the η mass. In Fig. 1 ROC model [4] predictions of the cross sections for a_0^+ production *together* with an estimate of the cross sections for the nonresonant and the multipion channels at the highest COSY energy are given. In these calculations the a_0^+ is considered as a usual quark model state with two decay channels $a_0^+ \to K^+\bar{K}^0$ and $a_0^+ \to \pi^+\eta$. The missing mass distributions of two particles are used to select the mass of the third particle defining thus the final channel. Then the signal from the a_0^+ is looked for in the missing mass distribution of the d. In case of strangeness production there are no background reactions, while channels with three or four pions may contribute to the η window in the $M_{d\pi}$ distribution. The difference between the full and the dotted histogram in the lower right panel of Fig. 1 is the contribution from these pion channels.

The main difficulty consists in differentiating between the channels via the a_0^+ meson and the channels with nonresonant production, especially in case of the channel $pp \to dK^+\bar{K}^0$, where the missing mass M_d varies only by about half the assumed width of the a_0^+ meson. The value of the calculated cross section for a_0^+ production is closely related to the assumption that the a_0^+ consists of light quarks. For the direct population of the channel $pp \to dK^+\bar{K}^0$ the creation of a $d\bar{d}$ and a $s\bar{s}$ pair is necessary. Strange quark production is suppressed and, therefore, the larger contribution to the final channel $dK^+\bar{K}^0$ comes from an intermediate a_0^+. In case of the decay channel, $a_0^+ \to \pi^+\eta$, the ROC model predicts higher cross sections for the nonresonant channel than for a_0^+ production. Therefore, the measurements should be carried out with high statistics.

References

[1] C. Caso et al., Eur. Phys. J. C 3 (1998) 1

[2] V. Y. Grishina et al., Eur. Phys. J. A 9 (2000) 2, 277, nucl-th/0007074

[3] V. Chernyshev et al., COSY Proposal #55: Study of a_0^+ mesons at ANKE (1997), cf. http://ikpd15.ikp.kfa-juelich.de:8085/doc/Anke.html

[4] H. Müller, Eur. Phys. J. C 18 (2001) 563, hep-ph/0011350

Tests of the First HADES Drift Chamber MDCIII [B,G,W]

R. Dressler, W. Enghardt, O. Fateev[1], E. Grosse, K. Heidel, J. Hutsch, R. Kotte, L. Naumann, M. Sobiella

The final design of the large trapezoidal low-mass drift chambers (MDCIII) of the HADES spectrometer tracking system has been performed at the detector laboratory of the FZ Rossendorf [1]. These drift chambers consist of 6 modules with an active area of 2.20 m^2 for each plane and a drift cell size of 8x12 mm^2. Each module has 6 drift cell layers, i.e. 6 anode and 7 cathode frames. The anode frames contain alternately signal wires (tungsten gold-coated, $\varnothing = 20\ \mu$m) and field wires (aluminium, $\varnothing = 100\ \mu$m) with a distance of 6 mm from each other. The wires in the anode frames have orientations of $-40°, +20°, -0°, +0°, -20°$ and $+40°$, respectively, whereas the wires in the cathode frames (aluminium, $\varnothing = 80\ \mu$m) have always the same orientation $+90°$ and a distance of 3 mm. Over the last two years we have solved all physical and technical problems of the design and production of the MDCIII. A full size prototype was finished in February 2000, consisting of only one anode frame (orientation $+0°$) between two cathode frames and in addition the other 10 frames without wires. Thus, the total volume of this prototype (150 l) matches the volume of a final MDCIII sector. A mixture of helium and iso-butan (60% He, 40% i-C_4H_{10}) was used for test measurements, which should be applied in real experiments. A stable gas mixture can be guaranteed by a flow of 10 l/h because the leakage rates of both gas components differ slightly (0.15 l/h at a level of 0.5 l/h). The results of first measurements are depicted in the following figures. Fig. 1. shows the current versus the high voltage. It is obvious to see, that external light sources (e.g. fluorescent tubes) dramatically reduce the break-through voltage, due to the emission of photo electrons from the Al wires.

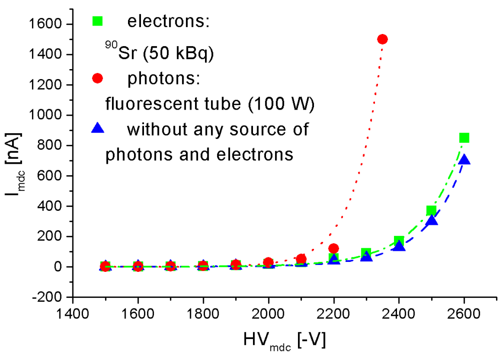

Fig. 1 *Current versus supplied high voltage for different working conditions.*

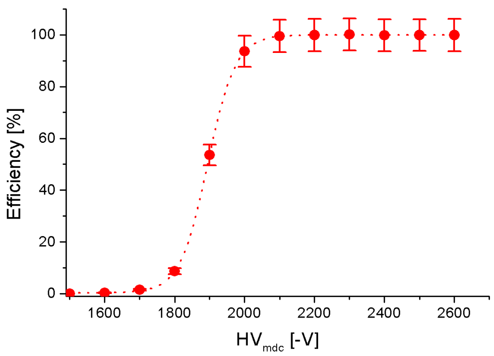

Fig. 2 *Counter efficiency versus supplied high voltage for the prototype.*

The counting characteristic of the prototype is depicted in Fig. 2. A ^{90}Sr source (50 kBq) was used to deliver electrons, which are additionally detected in a master scintillator telescope (20x20 mm^2), a 1 mm thick scintillator in front of the prototype and a 5 mm thick scintillator behind. The signal from the anodes was amplified by a factor of 50 with a fast current sensitive preamplifier [2] and further processed with NIM and CAMAC modules. Up to a high voltage of -2600 V the prototype works without break through. A large counting plateau of 500 V was found above -2100 V. Nearly hundred percent counter efficiency was reached for the individual drift layers and a value of 98% was determined for coincident signals in all six drift layers.

[1] *JINR, Dubna, Russia*

References

[1] http://www.fz-rossendorf.de/FWK/hp/hades.html
[2] K. Heidel et al., this Report

Status Report of the HADES Drift Chamber Read Out [B, G, W]

K. Heidel, R. Dressler, O. Fateev[1], R. Kotte, L. Naumann

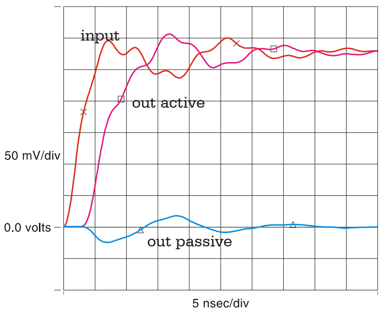

Fig. 1 *Crosstalk output active/passive (8%) for a 24 cm long PCB connector and a 27 cm long FPC cable.*

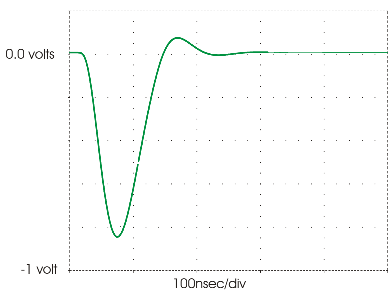

Fig. 2 *Simulated output signal for a 10 μA current signal and a detector capacity of 30 pF.*

The first module out of six multiwire drift chambers (MDC) designed for plane III of the HADES dielectron spectrometer [1] at GSI Darmstadt has been built and tested successfully [2]. The following report resumes the results of the electronics tests.

1. Simulation: In order to avoid secondary transmission line effects accurate pre-layout simulations, including crosstalk and reflection, have been performed for the printed circuit boards (PCB) developed to guide the signals from the MDC sense wires to the front-end electronics. The layout has been designed as a four-layer PCB with a thick dielectric between signal and ground layers and conductor widths of 0.1 mm to match the input impedance (Z_0 = 115 Ω) of the daughterboards (analog boards with ASD8 chips [3]). The simulation (cf. Fig. 1) yielded typical crosstalks of less than 8% for the common configuration of PCB and flex print cable (FPC [4]), where the latter one connects PCB and daughterboards. The capacity of MDC sense wire, PCB, and FPC, which is important for the input noise characteristics, was measured directly to be about 30 pF, depending on the wire length.

2. Pulse characteristics: A wire chamber acts as a current source with signals depending on the cell geometry, the gas filling and the electric field. A current-sensitive amplifier with a gain of dV_{out}/dI_{in} = 100 mV/μA has been developed [5] to match the small rise time of several ns (according to the collection time of electrons produced near to the sense wire) and the long fall time of about 50 - 100 ns (slow ion drift towards the cathode and field wires). Fig. 2 shows the result of the simulation for a 10 μA current signal. It is in agreement with the amplitude measured at the real amplifier output.

3. Concept of grounding: The front-end electronics consisting of daughterboards (incorporating the ASD8 chips with preamplifier, shaper, and discriminator; thus delivering logical time-above-threshold signals) and motherboards (carrying the TDC's to convert the information) is mounted at the edges of the detector frames. In order to obtain an optimum signal-to-noise ratio special attention has been payed to the grounding principle. The most effective grounding methods with respect to low noise level and small r.f. reception was figured out to be the following: 1) Using short flexible cables with high cross section, all PCB cards and also all analog and digital ground points of the daughterboards have been connected to a broad self-adhesive copper foil glued onto the frame below the motherboards. 2) A thick copper-track loop has been installed around the frame to conduct the reverse current (total 25 A!) back from the daughterboards and motherboards. With this arrangement an unrivaled low noise level of 20 mV (measured at the analog output of a daughterboard) without any disturbing r.f. crosstalk, e.g. arising from the 5 MHz quartz oscillator (clock) operating on the motherboard, has been attained.

[1] *JINR, Dubna, Russia*

References

[1] C. Müntz, for the HADES collaboration, Nucl. Phys. B 78 (1999) 139
[2] F. Dohrmann et al., this Report
[3] F.M. Newcomer et al., IEEE (1993) 630
[4] C. Müntz; http://www-hades.gsi.de/mdc/internal/techinfo/fpc/
[5] H. Langenhagen, FZ-Rossendorf, private information

First Beam Exposition of the HADES Drift Chamber MDCIII at SIS [B,G,W]

F. Dohrmann[1], R. Dressler, W. Enghardt, O. Fateev[2] E. Grosse, K. Heidel, K. Kanaki, R. Kotte, L. Naumann, M. Sobiella

The HADES spectrometer including all major detector units, read-out, data-acquisition and trigger electronics has been tested in the commissioning beam time in November 2000. It consists of ring imaging Cherenkov counters, multiwire drift chambers (MDC) of planes I to III, time of flight scintillation hodoscopes (TOF) and pre-shower modules [1]. The first large-area drift chamber MDCIII for the third tracking plane produced at FZ Rossendorf was installed in sector four of the HADES spectrometer (Fig. 1).
A 1.5 AGeV carbon beam with an intensity of 5×10^6 per spill hits a carbon target. The spill length amounted to 5 seconds. Most of the reaction products crossing the spectrometer were protons and pions. The chamber volume of 150 l has been filled with a gas mixture of 40% iso-butane and 60% helium at a flow rate of 10 l/h. The leakage rate was 0.5 l/h

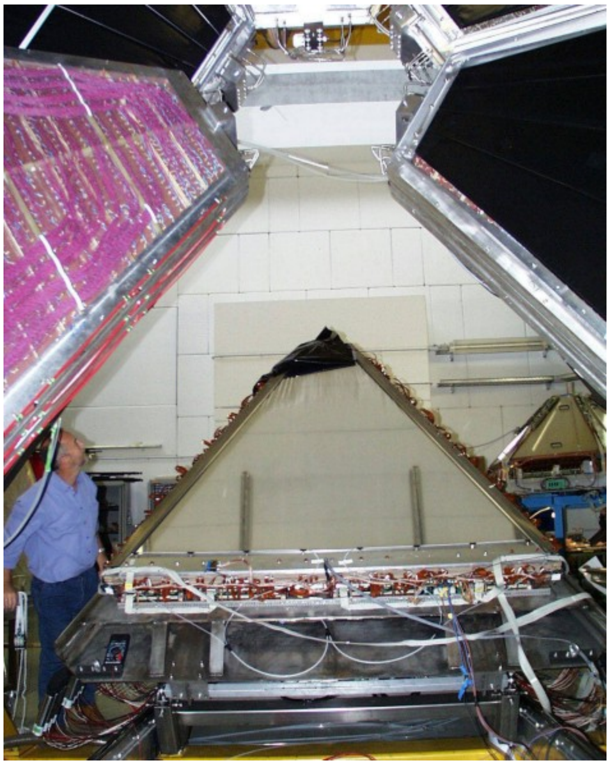

Fig. 1 *MDCIII mounted on the support frame of the HADES spectrometer. Under normal working condition the drift chambers are hidden inside the spectrometer core.*

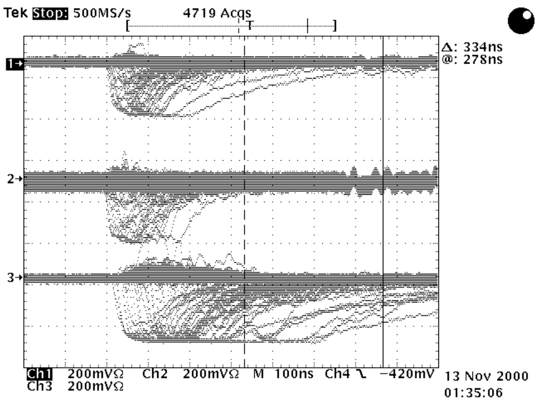

Fig. 2 *The analog signals monitored with a scope. The signals shown from top to bottom were measured on MDC planes I to III.*

The applied high voltage amounts to -2 kV for both the cathode and field wires. A selected anode wire is connected to an analog output to check the amplified signals as shown in Fig. 2. The shape of the signal shows a risetime of 30 ns up to the saturation level of the preamplifier.
The MDCIII is equipped with dedicated preamplifier/shaper/discriminator boards inserted into motherboards which itself contain the digitizers (TDC). These daughter- and motherboard components are mounted onto the detector frame under accurate consideration of the grounding [3].

The data acquisition was triggered by the TOF multiplicity $\geq$ 4. A typical TDC spectrum is shown in Fig. 3. The drift velocity was estimated to be 33 μm/ns based on a drift time distribution of 180 ns (FWHM) and the lateral half cell size of 6 mm. There is no visible effect of the strong magnetic field (0.2 T), created by superconducting solenoids in front of the MDCIII, onto the drift time spectrum.

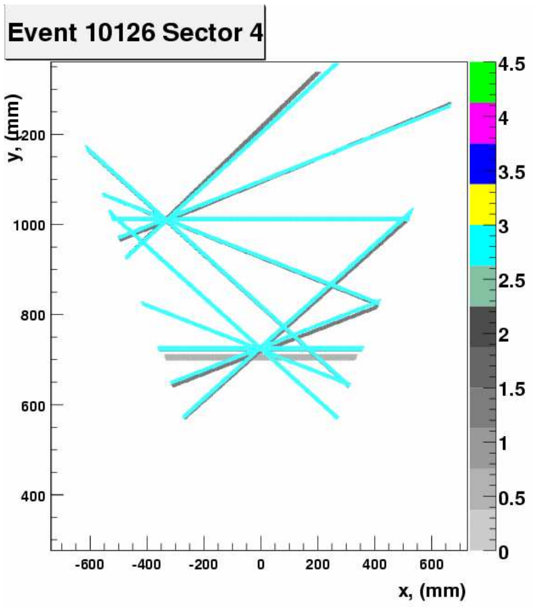

Fig. 4 *Two prongs of an event align between the target and the points of intersection in all three MDC's of sector four (bottom) of the HADES spectrometer. Each prong is characterised by the point of intersection of all fired signal wires in the two dimensional projection plane. The MDC plane numbers have been labeled by colors.*

[1] *ANL, Argonne, USA*
[2] *JINR, Dubna, Russia*

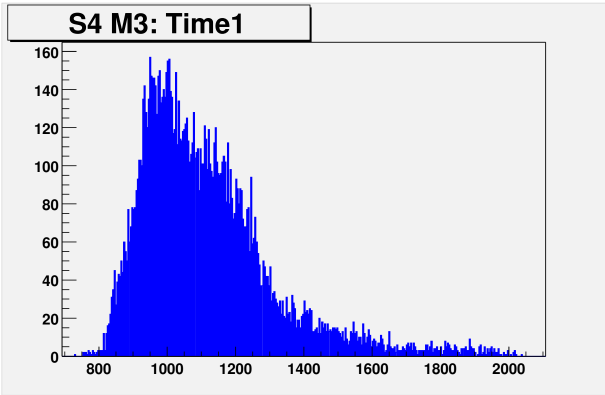

Fig. 3 *Drift time distribution of leading electrons in one anode layer of MDCIII (0.5 ns/channel). The time measurement started by a common signal, created by the TOF trigger, and stopped by an individual anode signal.*

A stereo optical positioning system [2] monitors with a resolution of 1 μm the three dimensional displacement between the MDC's before and behind the magnet. The mean observed displacement during all runs was less than 10 μm.
Fig. 4 shows as a highlight of the commissioning, a plot of the reconstruction of the linear flight paths of charged particles through three MDC planes without magnetic field. In each drift chamber the hit trajectory is defined by at least five anode layers giving a coincident signal. The hit positions have been defined by the dimensions of the drift cells only. The drift time information is not used for this plot.

References

[1] http://www-hades.gsi.de
[2] H. Alvarez-Pol, privat information
[3] K. Heidel et al., this Report

Probing the Vector Meson Spectral Function by Multidifferential Cross Sections B,W

B. KÄMPFER, O.P. PAVLENKO[1], GY. WOLF[2]

The starting experimental programme at the new detector facility HADES at SIS/GSI Darmstadt offers the access to dileptons in various reactions of heavy ions and hadrons (pions and protons) with various nuclear targets. One motivation of such experiments is the study of the in-medium change of the vector meson spectral functions. Within various models vastly different predictions are available ranging from a simple shift of the pole position of the spectral function to a strong broadening up to a fragmentation due to particle-hole excitations caused by the ambient matter.

While a moderate broadening of the most sensitive ρ meson spectral function leads probably to a disappearance of the ρ peak in the invariant mass spectrum $d\sigma/dM^2$, we have shown in [1] that, within a schematic blast wave model, measuring the double differential cross section $d\sigma/dM^2 dM_\perp^2$ in a sufficiently restricted interval of the transverse mass $M_\perp$ as function of the invariant mass M still allows to identify the ρ signal. As an example, in Fig. 1 the dilepton emission rate is displayed. Here, we assumed that the widths of the vector mesons are increased by a factor of 3 due to in-medium effects. Indeed, while in the invariant mass spectrum the ρ peak is not longer visible, selecting an narrow interval of values of $M_\perp$ the ρ is clearly seen.

This feature is persistent when integrating the rate over the space-time history of the radiating matter. Additional complications arise due to the suspected strong coupling of the widths and pole positions to the baryon density and temperature, which change in space and time.

Employing a transport calculation of BUU type we have checked that such background contributions as pn bremsstrahlung, η Dalitz and Δ Dalitz decays are sufficiently strongly suppressed when selecting the interval 850 MeV $< M_\perp <$ 950 MeV. The count rates for this range of $M_\perp$ are not too small to make such measurements feasible.

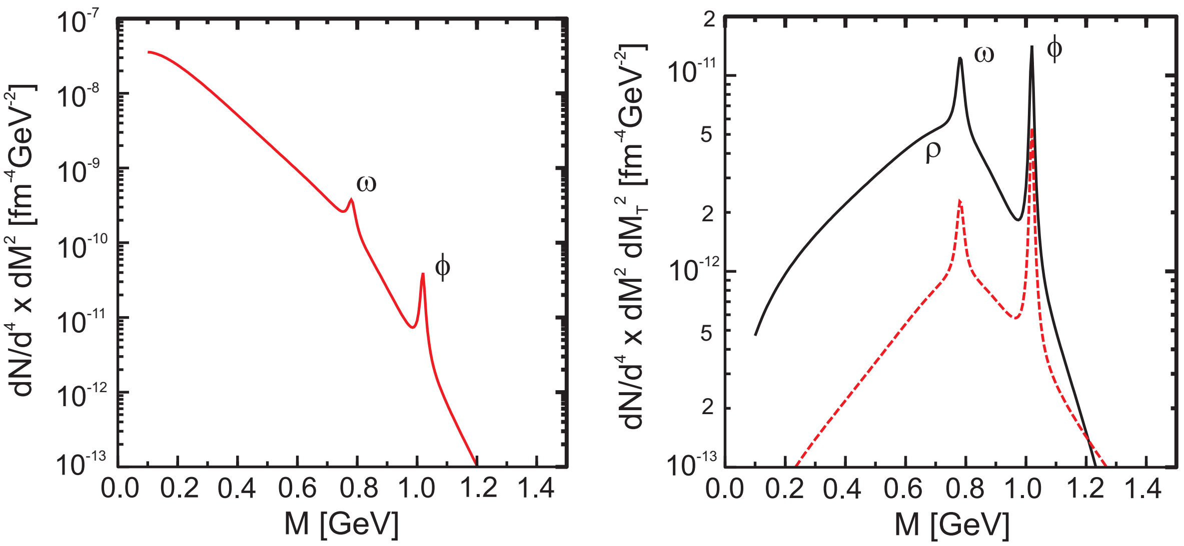

Fig. 1 *The dilepton emission rates $dN/(d^4x\,dM^2)$ (left panel) and $dN/(d^4x\,dM_\perp^2\,dM^2)$ (right panel, $M_\perp = 1.3$ GeV) for $T = 70$ MeV and radial expansion velocities of $v_r = 0.1$ (dashed curve) and 0.3 (solid curve).*

[1] *Institute of Theoretical Physics, Kiev, Ukraine*
[2] *KFKI Budapest, Hungary*

References

[1] B. Kämpfer, O.P. Pavlenko, Eur. Phys. J. A 10, 101 (2001)

Analysis of Dilepton Data from Heavy–Ion Experiments at CERN–SPS [B,W]

K. Gallmeister, B. Kämpfer, O.P. Pavlenko[1], C. Gale[2]

An excess of dileptons in lead–beam induced heavy–ion collisions has been reported (i) by the CERES collaboration in the low–mass region of dielectrons and (ii) by the NA50 collaboration in the intermediate–mass region of dimuons. This excess points to the existence of a system of thermalized matter emitting dileptons [1].
We achieve a good description of the mentioned data by a superposition of the thermal yield and either the hadronic cocktail in case of CERES data or both the contributions from correlated semileptonic decays of open charm mesons and the Drell–Yan process for NA50 data (see figs. 1 and 2 and [1] for details).
The thermal source is characterized by a mean temperature $\langle T \rangle = 170$ MeV. A similar value is found in an analysis of the dilepton data of the CERES, Helios/3 and NA38 collaborations with the sulfur beam [2]. In the dynamic scenario we find an initial temperature of the thermal system in the order of 200 MeV, i.e. a value larger than the expected deconfinement temperature.

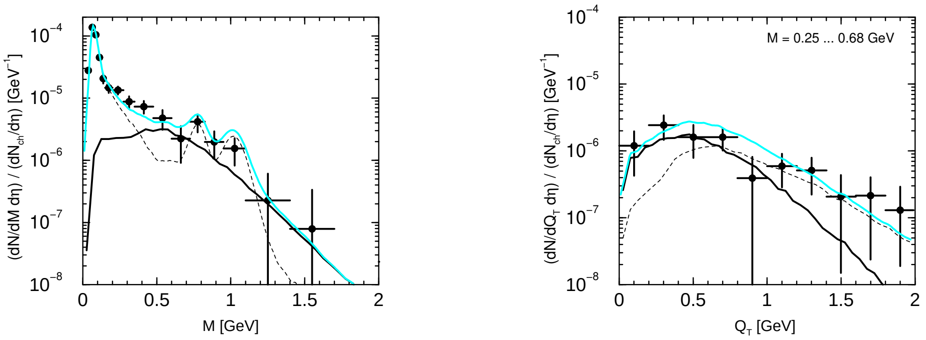

Fig. 1 *A comparison of our model with the CERES data. The dashed curves are the hadronic cocktail published by the CERES collaboration, the solid curves are the contributions from the thermal system. The sum is depicted by the gray curves. Left panel: the invariant mass spectrum, right panel: the transverse momentum spectrum for the invariant mass region $M = 0.25 \ldots 0.68$ GeV.*

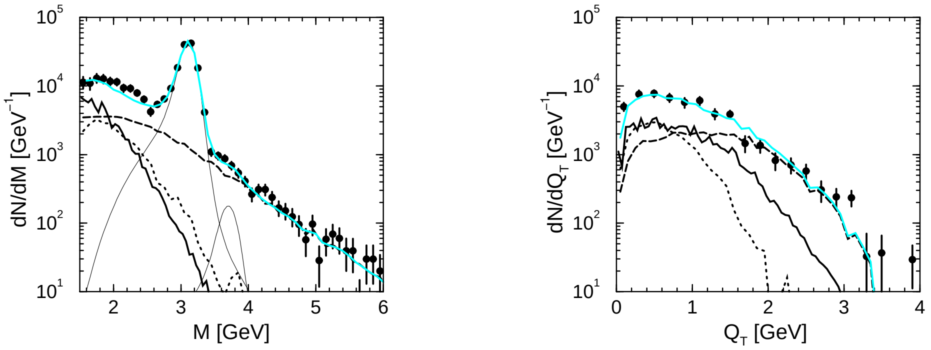

Fig. 2 *The data of the NA50 collaboration for the invariant mass spectrum (left) and the transverse momentum spectrum in the invariant mass region $M = 1.5 \ldots 2.5$ GeV (right). The dashed curves are the Drell–Yan contributions, the dotted curves show the contributions of open charm and the solid lines depict the yield of the thermal system. The sum is shown by the gray curves.*

[1] *Institute for Theoretical Physics, 252143 Kiev - 143, Ukraine*
[2] McGill University, Montreal, QC, H3A 2T8, Canada

References

[1] K. Gallmeister, B. Kämpfer, O.P. Pavlenko, Phys. Lett. B 473, 20 (2000)
[2] K. Gallmeister, B. Kämpfer, O.P. Pavlenko, C. Gale, Nucl. Phys. A 688, 933 (2001)

Analysis of the Direct Photon Data of the Experiment WA98 [B,W]

K. Gallmeister, B. Kämpfer, O.P. Pavlenko[1]

Recently the WA98 collaboration published data concerning the direct photon production in the reaction $Pb(158\ \mathrm{A}GeV) + Pb$ [1]. Analog to our studies [2] of the dilepton spectra in similar reactions, we use a superposition of hard photon production processes and of the yields from thermalized matter in order to describe these data.

The contributions of the hard annihilation and Compton like diagrams within the framework of perturbative QCD are calculated using the event generator PYTHIA. The comparison of PYTHIA results and various direct photon data in proton induced collisions indicates that the shapes of the data are well described. Fig. 1 displays two examples of the comparison of our calculations and data.

The hard perturbative QCD contribution, calculated for pp collisions, is up–scaled such that the large–$p_\perp$ tail of the WA98 data is reproduced (cf. fig. 2). The thermal source is described by

$$\frac{dN}{d^3p/E} = N_{\mathrm{eff}}\, \frac{5\alpha\alpha_s T_{\mathrm{eff}}^2}{12\pi^2} \int_0^1 ds\ s^2 \int_{-1}^{+1} d\xi\ e^{-A} \log\left[1 + \frac{2.912}{4\pi\alpha_s} A\right] \tag{9}$$

with $A = \frac{p_\perp \cosh y\,(1 - s v_0 \xi)}{T_{\mathrm{eff}}\sqrt{1-(s v_0)^2}}$, an effective temperature of $T_{\mathrm{eff}} = 170$ MeV and a space–time normalization factor $N_{\mathrm{eff}} = 3 \times 10^4$ fm^4. These parameters are taken from our analysis [2] of dilepton data. Contrary to the SPS dilepton data, flow effects are visible in the photon $p_\perp$ spectra at values around 2 GeV. With a maximal radial expansion of $v_0 = 0.3c$ of the radiating fireball a good description of the data is achieved (see fig. 2).

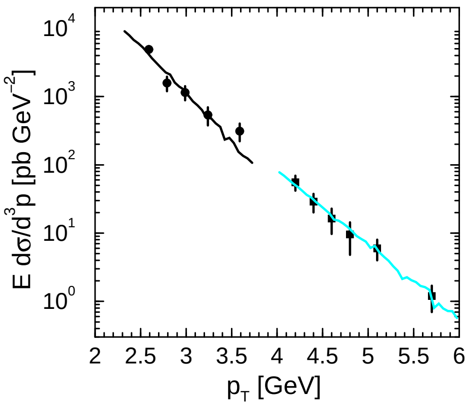

Fig. 1 *A comparison of calculations of the hard photon production in proton–proton collisions with data from E704 [3] at $\sqrt{s} = 19.4$ GeV (small $p_\perp$ values) and from UA6 [4] at $\sqrt{s} = 24.3$ GeV (large $p_\perp$ values). For more details cf. [5].*

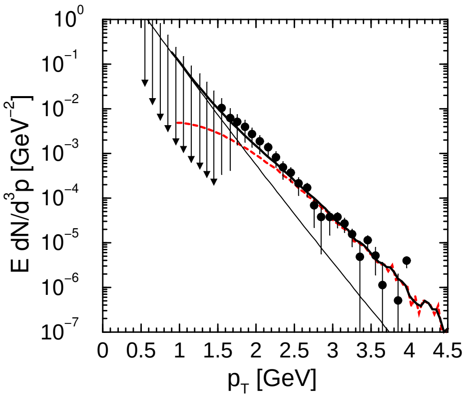

Fig. 2 *The data of the WA98 collaboration [1] compared with the hard direct photons (dashed curve) and the thermal contribution (thin curve). The sum of these contributions is depicted by the solid curve. A radial flow of $v_0 = 0.3c$ is assumed.*

[1] *Institute for Theoretical Physics, 252143 Kiev - 143, Ukraine*

References

[1] M. M. Aggarwal et al. (WA98), Phys. Rev. Lett 85 (2000) 3595
[2] K. Gallmeister, B. Kämpfer, O.P. Pavlenko, Phys. Lett. 473 (2000) 20
[3] D.L. Adams et al. (E704), Phys. Lett. B 345 (1995) 569
[4] G. Ballocchi et al. (UA6), Phys. Lett. B 317 (1993) 250
[5] K. Gallmeister, B. Kämpfer, O.P. Pavlenko, Phys. Rev. C 62 (2000) 057901

Solar Proton Burning Process Revisited [B,W]

L.P. Kaptari[1], B. Kämpfer, E. Grosse

Recently the solar proton burning process, $pp \to e^+ \nu_e D$, has been revisited by various authors since the previous canonical value of the corresponding S_{pp} factor has been questioned. This stimulated us to calculate the relevant matrix elements within a fully covariant model of the deuteron D, based on the Bethe-Salpeter (BS) formalism. The relevant Feynman type diagrams are displayed in Fig. 1. Within our approach [1] a variety of quantities, including the total and differential cross sections, energy dependences, angular distributions etc. are accessible. Within the relativistic impulse approximation a covariant expression for the S_{pp} factor is obtained (see Fig. 2). Our result confirms the old canonical value of $S_{pp} \approx 4.00 \times 10^{-25}$ MeV b, which is in agreement with the energy balance of the sun and helioseismic data.

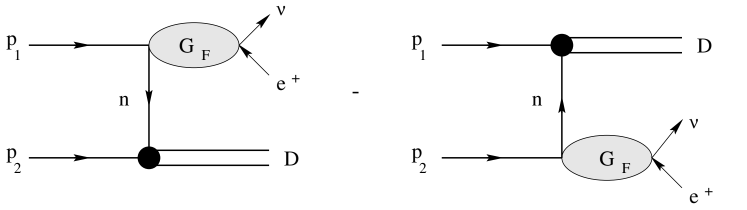

Fig. 1 *Feynman diagrams contributing to the processes $pp \to e^+ \nu D$.*

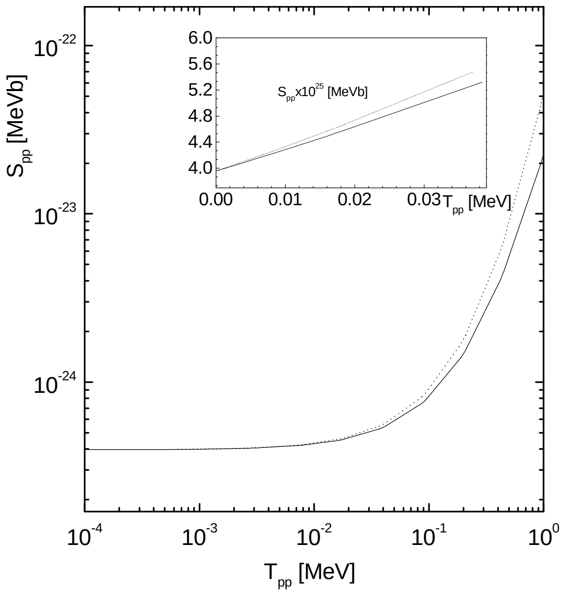

Fig. 2 *The S_{pp} factor for the reaction $pp \to e^+ \nu D$ as a function of the relative kinetic energy of incident protons, T_{pp}. The solid line is the result of a calculation by using the full deuteron wave function, while the dotted line is the result of a computation with the deuteron wave function taken as constant (for details consult [1]). The inset shows S_{pp} vs. T_{pp} in linear scales.*

Encouraged by the applicability of our approach we have also studied the reaction $e^+ D \to pp\bar{\nu}_e$ representing a cross channel of the solar burning process. In principle, such a reaction is feasible under laboratory conditions. For instance, at ELBE also a positron source is planned. However, the calculated cross section is exceedingly small. The competing electromagnetic deuteron disintegration reactions, $e^{\pm} D \to e^{\pm} pn$, have cross sections many orders of magnitude above the interesting weak disintegration process. Therefore, due to severe background problems, a dedicated experimental investigation of the astrophysically interesting weak deuteron disintegration seems to be far out of reach.

[1] *Bogolyubov Laboratory of Theoretical Physics, JINR Dubna, Russia*

References

[1] L. P. Kaptari, B. Kämpfer, E. Grosse, J. Phys. G 26 (2000) 1423